Improved representation of isoprene-derived secondary organic aerosol in CAM6-Chem reveals regional contrasts in its long-term changes over China

Wenxin Zhang[1], Man Yue[1,2], Xinyue Shao[1], Xinyi Dong[1,3,4], Minghuai Wang[1,4]

[1]School of Atmospheric Science, Nanjing University, Nanjing, 210023, China
[2]Zhejiang Institute of Meteorological Sciences, Hangzhou, 310008, China
[3]Frontiers Science Center for Critical Earth Material Cycling, Nanjing University
[4]Joint International Research Laboratory of Atmospheric and Earth System Sciences & Institute for Climate and Global Change Research, Nanjing University, Nanjing, 210023, China

Correspondence to: Xinyi Dong (dongxy@nju.edu.cn)

Abstract. Isoprene-derived secondary organic aerosol (ISOA) is an important component of atmospheric organic aerosol, but its formation remains incompletely represented in global chemical models, creating uncertainty in ISOA changes and their drivers. In this study, we implemented an explicit ISOA formation scheme in Community Atmosphere Model version 6 with comprehensive tropospheric and stratospheric chemistry (CAM6-Chem), incorporating high-NOx gas-phase epoxide precursors and explicitly representing branch-resolved heterogeneous uptake from both low-NOx and high-NOx pathways~~In this study, we updated the explicit isoprene chemistry scheme in Community Atmosphere Model version 6 with comprehensive tropospheric and stratospheric chemistry (CAM6-Chem) by adding isoprene epoxydiols reactive uptake to aerosol liquid water under low-NOx conditions and key gas-phase precursors and subsequent heterogeneous processes under high-NOx conditions~~. Evaluation against ground-based observations shows that the updated model reasonably reproduces the concentrations and compositional structure of four explicitly represented ISOA subspecies.~~Evaluation against ground-based observations shows that the updated model better reproduces the concentrations and compositional structure of four ISOA subspecies, rather than only one in the default model.~~ At the bulk aerosol level, the update alleviates the underestimation of SOA over China, improving normalized mean bias from −76.7% to −~~50.0~~51.6%. ISOA formation in China is governed by NOx-dependent competition between the low- and high-NOx pathways, with the former remaining dominant at the national scale. Long-term analysis for 2000–2019 shows a weak national-mean ISOA trend due to offsetting regional changes of opposite signs. The most pronounced increase occurs in Southwest China, where enhanced biogenic isoprene emissions emerge as the leading statistical predictor of the ISOA increase, with a regression-based relative contribution of ~~61.92~~58.29%. The strongest decrease occurs in the Shaanxi–Gansu–Ningxia region, where declining sulfate is identified as the leading statistical predictors, with regression-based relative contributions of 63.37%.~~The strongest decrease occurs in the Shaanxi–Gansu–Ningxia region, where increasing anthropogenic nitrogen oxides (NOx) emissions and declining sulfate are identified as the two leading statistical predictors, with regression-based relative contributions of 48.96% and 45.11%, respectively.~~ These results highlight the regional heterogeneity of ISOA changes in China and the

importance of jointly representing precursor supply and heterogeneous reaction conditions in simulating ISOA formation and trends.

1 Introduction

Isoprene (C_5H_8) is one of the most important biogenic volatile organic compounds (VOCs) in the atmosphere, with global emissions accounting for nearly half of the total biogenic VOC emissions (Guenther et al., 2012). Owing to its very high chemical reactivity, isoprene is rapidly oxidized in the atmosphere by hydroxyl radicals (OH), ozone (O_3), and nitrate radicals (NO_3) (Wennberg et al., 2018). The resulting oxidation products can further undergo multiphase chemical processes to form secondary organic aerosol (SOA) with semi-volatile and low-volatility characteristics.

The mechanisms by which isoprene forms SOA are highly sensitive to the ambient nitrogen oxides (NOx) background (Surratt et al., 2010). Under low-NOx conditions, the primary oxidation products of isoprene readily react with hydroperoxyl radicals (HO_2) or organic peroxy radicals (RO_2) to form isoprene hydroxyl hydroperoxides (ISOPOOH), as well as carbonyl and hydroxylated products (Wennberg et al., 2018). ISOPOOH is further oxidized by OH under low-NOx conditions to produce isoprene epoxydiols (IEPOX), with a molar yield exceeding 75% (Paulot et al., 2009b). Hereafter, this low-NOx sequence is referred to as the IEPOX pathway. IEPOX is highly water-soluble and reactive, and it can undergo acid-catalyzed multiphase processing to form SOA (Lin et al., 2012; Surratt et al., 2010). In these heterogeneous reactions, aerosol liquid water, sulfate, and nitrate can all act as key nucleophiles that add to the epoxide upon ring opening, producing low-volatility products. Specifically, aerosol liquid water-mediated pathways form 2-methyltetrols (2-MT) and related polyols, whereas sulfate- and nitrate-mediated nucleophilic addition produces organosulfates, organonitrates, and other oligomeric products that contribute substantially to SOA formation (Paulot et al., 2009b; Surratt et al., 2007, 2008, 2010). Under high-NOx conditions, the primary oxidation products of isoprene preferentially react with nitric oxide (NO) to form important gas-phase intermediates such as methacryloyl peroxynitrate (MPAN) (Wennberg et al., 2018). Subsequent reactions of these intermediates with OH can produce epoxides, including methacrylic acid epoxide (MAE) and hydroxymethyl-methyl-α-lactone (HMML) (Lin et al., 2013; Nguyen et al., 2015). After partitioning into the particle phase, these epoxides undergo acid-catalyzed ring opening and subsequent multiphase processing, in which aerosol liquid water, sulfate, and nitrate act as important nucleophiles. These reactions ultimately yield SOA components dominated by 2-methylglyceric acid (2-MG), organosulfates, and organonitrates (Birdsall et al., 2014; Nguyen et al., 2015; Schwantes et al., 2019). Hereafter, this high-NOx sequence is referred to as the MAE/HMML pathway. Although observational studies indicate that ambient concentrations of MAE and HMML are generally lower than those of IEPOX under low-NOx conditions (Worton et al., 2013; Zhu et al., 2025), they remain key precursors for ISOA formation in high-NOx environments and play a non-negligible role in the isoprene oxidation system. In regions strongly influenced by human activities (e.g., urban and industrial areas), NOx concentrations are elevated while isoprene emissions remain substantial,

making this pathway more influential for ISOA formation in such environments (Budisulistiorini et al., 2015; Rattanavaraha et al., 2016).

To improve model performance and simulation accuracy, it is essential to better represent ISOA formation across different NOx regimes.~~incorporate the high-NOx pathway~~. The high-NOx pathway remains insufficiently represented in global models, which can contribute to the underestimation of ISOA in polluted regions~~Its absence in most global models has contributed to the underestimation of ISOA in high-NOx regions~~ (Budisulistiorini et al., 2015; Hu et al., 2015; Lin et al., 2013). Observational evidence suggests that this pathway can contribute about 13–26% of ISOA in urban environments, highlighting its importance under polluted conditions (Ding et al., 2014; Zhang et al., 2022). Equally important is a product-level representation of IEPOX-derived ISOA ($ISOA_{IEPOX}$), rather than representing it as a single lumped product, because major molecular tracers such as 2-MT and organosulfate/organonitrate products provide important constraints on ISOA composition and particle-phase processing (Chen et al., 2024b; Lin et al., 2012). ~~Equally important is an explicit treatment of IEPOX multiphase chemistry, including reactions in aerosol liquid water, because 2-MT are formed through particle-phase hydrolysis following epoxide ring opening and are widely used as major molecular tracers of IEPOX-derived ISOA ($ISOA_{IEPOX}$) (Chen et al., 2024b; Lin et al., 2012).~~ Therefore, explicitly representing key ISOA subspecies from both low-NOx and high-NOx epoxide pathways provides a more complete description of ISOA formation across pollution regimes.~~Therefore, representing both the MAE/HMML pathway under high-NOx conditions and the IEPOX plus aerosol liquid water branch under low-NOx conditions provides a more complete description of ISOA formation across pollution regimes,~~ improves the simulation of ISOA composition, and enhances the model sensitivity to changes in anthropogenic emissions.

ISOA plays a key role at the interface of natural and anthropogenic emissions and has received wide attention in recent years (Marais et al., 2016; Shrivastava et al., 2019, 2022). ISOA formation is jointly influenced by precursor emissions, oxidative environment, and meteorological conditions, leading to significant temporal and spatial variability (Bardakov et al., 2021; Carlton et al., 2009). Over the past two decades, rapid economic development across various regions and the continuous implementation of different pollution control measures have led to significant changes in both anthropogenic pollutant emissions and meteorological conditions, resulting in notable trends in ISOA concentrations (Silver et al., 2020; Su et al., 2011; Zhang et al., 2025). Therefore, it is important to further investigate the key factors and mechanisms driving these concentration changes. Existing studies on ISOA concentration changes have predominantly focused on the IEPOX pathway, where sulfate has been identified as a key driver of variability. For instance, Marais et al. (2017) found that, during 1991–2013, $ISOA_{IEPOX}$ in the United States decreased significantly with declining sulfate, making sulfate the primary driver of the long-term summertime reduction in surface organic aerosol (OA) (Marais et al., 2017). Similarly, long-term simulations by Zheng et al. (2020) confirmed a 4.9% per year decrease in $ISOA_{IEPOX}$ in the southeastern United States from 2000 to 2013, attributed primarily to sulfate reductions (Zheng et al., 2020). This finding was consistent with Dong et al. (2022), who

showed that sulfate reductions in southern China corresponded to declines in $ISOA_{IEPOX}$ (Dong et al., 2022). Zhang et al. (2025) also reported that sulfate decreases across China were accompanied by a decline in $ISOA_{IEPOX}$ (Zhang et al., 2025). Liu et al. (2023) also observed that decreasing sulfate emissions contributed significantly to the decline in $ISOA_{IEPOX}$ over the continental United States based on long-term model simulations (Liu et al., 2023). However, some studies that consider the MAE/HMML pathway report different results, indicating that the dominant drivers of ISOA can vary by region and environment. For instance, Hu et al. (2025) showed that in Shanghai during 2015–2021, anthropogenic NOx emissions were the primary driver of ISOA reduction, with sulfur dioxide (SO_2) and aerosol acidity playing secondary roles (Hu et al., 2025). Similarly, Budisulistiorini et al. (2015) found in the 2013 Southern Oxidant and Aerosol Study that human pollution significantly influenced both the IEPOX and MAE/HMML pathways, with sulfate and NO_3 affecting their relative importance in urban areas (Budisulistiorini et al., 2015).

Despite these advances, existing studies still rarely assess long-term ISOA changes by simultaneously considering pathway competition under different NOx emission backgrounds and the multiphase reaction environment. Given the large regional contrasts in emissions, meteorological conditions, and oxidation environments across China (Ding et al., 2016; Li et al., 2018; Wu et al., 2020; Yang et al., 2017), the dominant factors controlling ISOA formation and change are likely to differ by region. To further explore this question, a model framework is needed that can represent both low-NOx and high-NOx epoxide pathways and distinguish their major reaction branches and products. The continuous development of SOA representation in large-scale models provides an important foundation for this purpose. Representations of biogenic SOA have evolved from simplified empirical or fixed-yield treatments used in early global models (Chung and Seinfeld, 2002; Chin et al., 2002; Carlton et al., 2010; Kim et al., 2015), through semi-empirical two-product absorptive partitioning models (Odum et al., 1996; Griffin et al., 1999), to volatility-based gas-particle partitioning schemes (Donahue et al., 2006; Robinson et al., 2007; Pye and Seinfeld, 2010), and more recently to explicit multiphase reactive uptake parameterizations for isoprene epoxides (Pye et al., 2013; Budisulistiorini et al., 2017; Jo et al., 2019, 2021; Ng et al., 2025). These developments allow ISOA formation to respond more directly to aerosol liquid water, acidity, sulfate, and other nucleophiles, and particle-phase reaction kinetics (Pye et al., 2013; Marais et al., 2016; Budisulistiorini et al., 2017; Jo et al., 2019, 2021). Building on this progress, this study extends the CAM6-Chem framework by incorporating high-NOx epoxide precursors and subsequent heterogeneous reactions, distinguishing between H_2O-mediated nucleophilic addition and inorganic-nucleophile addition product classes, and evaluating how these updates affect ISOA composition and long-term ISOA trends over China. This framework further allows us to examine how ISOA trends are jointly controlled by precursor supply and heterogeneous reaction capacity across different regions. Nevertheless, important uncertainties remain in the current ISOA framework, including the simplified core-shell treatment of epoxide reactive uptake, uncertainties in aerosol phase state, organic-shell viscosity, phase separation, and diffusion limitations, as well as limited kinetic constraints for HMML/MAE uptake. Additional uncertainties arise from the assumptions of 100% SOA yield and non-volatile epoxide-derived products, and from the possible omission of non-epoxide ISOA pathways in the current framework. Despite these remaining

uncertainties, clarifying regional ISOA trends and controls can provide a scientific basis for evaluating how emission reductions jointly affect precursor supply and heterogeneous reaction environments, and for developing more targeted regional air-quality management strategies.~~Despite these advances, existing studies still rarely assess long-term ISOA changes by simultaneously considering pathway competition under high-NOx conditions and the aerosol liquid water branch of IEPOX chemistry. Given the large regional contrasts in emissions, meteorological conditions, and oxidation environments across China, the dominant factors controlling ISOA formation and change are likely to differ by region. Therefore, a more complete model representation that includes both high-NOx pathways and the IEPOX plus aerosol liquid water branch is needed to characterize the long-term evolution of ISOA across China and to identify the dominant drivers in different regions. Clarifying these regional trends and controls can also provide a scientific basis for evaluating the synergistic effects of emission reduction measures on SOA and for developing more targeted regional air-quality management strategies.~~

2 Data and Methods

2.1 Model Description

2.1.1 Model Configuration

This study employs the Community Atmosphere Model version 6 with comprehensive tropospheric and stratospheric chemistry (CAM6-Chem) within the Community Earth System Model version 2.1.0 (CESM2.1.0). Biogenic emissions are calculated online using the Model of Emissions of Gases and Aerosols from Nature version 2.1 (MEGAN2.1), which is coupled to CESM (Emmons et al., 2020; Guenther et al., 2012). Anthropogenic emissions are taken from the Multi-resolution Emission Inventory for China (MEIC; http://www.meicmodel.org) (Li et al., 2017). In this study, intermediate-volatility organic compounds (IVOCs) and semi-volatile organic compounds (SVOCs) represent lumped lower-volatility organic precursor classes defined by volatility rather than explicitly speciated molecular structures. Emissions of ~~intermediate-volatility organic compounds (~~IVOCs~~)~~ and ~~semi-volatile organic compounds (~~SVOCs~~)~~ are scaled from primary organic aerosol (POA) and non-methane volatile organic compounds (NMVOCs) emissions (Chang et al., 2022; Tilmes et al., 2019). The specific scaling equations and coefficients are described in the supplement of Zhang et al. (2025) (Eqs. A1–A3). Meteorological fields are constrained by the Modern-Era Retrospective analysis for Research and Applications (MERRA2) reanalysis data (Gelaro et al., 2017).

Gas-phase chemistry follows MOZART-TS2 (Model of Ozone And Related chemical Tracers, Troposphere–Stratosphere V2), including comprehensive isoprene and monoterpenes chemistry (Schwantes et al., 2020). Aerosols are represented using the four-mode version of the Modal Aerosol Module (MAM4) (Liu et al., 2016). This study employs two different approaches to treat SOA formation. First, the Volatility Basis Set (VBS) approach (Donahue et al., 2006; Hodzic et al., 2016) represents the gas–particle interconversion of organic compounds. Organic compounds (including glyoxal, monoterpenes,

sesquiterpenes, benzene, toluene, lumped xylenes, IVOCs, and SVOCs) are oxidized to form gas-phase SOA precursors in five volatility bins, with effective saturation concentrations (C*, at 300 K) of 0.01, 0.1, 1.0, 10.0, and 100.0 μg m^{-3}. These precursors subsequently partition between the gas and particle phases (Tilmes et al., 2019).~~VOCs (including glyoxal, monoterpenes, sesquiterpene, benzene, toluene, lumped xylenes, IVOCs, and SVOCs) are oxidized to five different types of volatile SOA gaseous precursors, with effective saturation concentrations (C*, at 300 K) of 0.01, 0.1, 1.0, 10.0, and 100.0 μg m^{-3} (Tilmes et al., 2019).~~ This VBS treatment follows the default CAM6-Chem SOA scheme and was not modified in this study. Second, SOA formation from isoprene gas phase products is treated explicitly (Sect. 2.1.2). In addition to ISOA, all other SOA are simulated using the VBS approach. Photolysis rates for monoterpene-derived SOA were updated based on our previous work (Liu et al., 2023). Aerosol wet removal scheme uses the Cloud Layers Unified By Binormals (CLUBB) scheme to provide a unified treatment of shallow convection and stratiform clouds, coupled with the two-moment cloud microphysics scheme by Gettelman and Morrison (2015) (MG2) to represent aerosol activation and removal (Gettelman and Morrison, 2015). This study adopts the Zhang and McFarlane (1995) (ZM95) parameterization for deep convective clouds and treats aerosol wet scavenging using empirical coefficients (Zhang & McFarlane, 1995).

The earlier CAM6-Chem configuration described by Zhang et al. (2025) represents ISOA formation mainly through the low-NOx pathway, in which $ISOA_{IEPOX}$ is treated as a lumped product. This lumped low-NOx representation limits the model's ability to describe ISOA formation across different NOx regimes and to distinguish product-level responses to changes in the particle-phase reaction environment. To address this limitation, Sect. 2.1.2 describes the explicit ISOA representation adopted in this study. This explicit representation incorporates high-NOx epoxide precursors and their subsequent heterogeneous uptake, allowing the model to characterize ISOA formation in urban and polluted regions where the high-NOx pathway can contribute substantially to total ISOA. It also resolves reactive-uptake-derived ISOA into product classes formed via H_2O-mediated nucleophilic addition and inorganic-nucleophile addition, thereby improving the model's ability to represent ISOA compositional changes associated with aerosol liquid water, inorganic nucleophiles, and acidity. Overall, this explicit ISOA formation mechanism enhances the model's sensitivity to changes in anthropogenic emissions and climate conditions. ~~The current model version is based on that used in Zhang et al. (2025), but its representation of isoprene chemistry remains incomplete. First, key gas-phase reactions under high-NOx conditions and their major intermediates, HMML and MAE, are not explicitly represented. Second, the heterogeneous chemistry has only accounted for the reactive uptake of IEPOX by sulfate and nitrate. It lacks the aerosol liquid water reaction branch of IEPOX and a consistent multiphase treatment of high-NOx products, including HMML and MAE. These limitations may constrain the model's applicability in urban and polluted regions and weaken its sensitivity to changes in anthropogenic emissions and the chemical environment. Therefore, Sect. 2.1.2 introduces the gas-phase and heterogeneous processes newly implemented in this study.~~

2.1.2 New processes added to isoprene chemistry

Under low-NOx conditions, the MOZART-TS2 gas-phase mechanism is retained, in which ISOPOOH reacts with OH to produce IEPOX with a molar branching ratio of 0.85. Under high-NOx conditions, following Lin et al. (2013), the gas-phase isoprene chemistry is expanded to explicitly represent MPAN and its subsequent reaction with OH (Lin et al., 2013). Methacrolein (MACR), the precursor of MPAN in the high-NOx pathway, is formed following the default MOZART-TS2 mechanism. The reaction of MPAN with OH yields HMML and MAE, with molar branching ratios of 0.75 and 0.02, respectively, based on the experimental results reported by Nguyen et al. (2015) (Table S2).~~MACR formation follows the default MOZART-TS2 mechanism. The reaction of MPAN with OH yields HMML and MAE, with molar branching ratios of 0.57 and 0.21, respectively.~~ No explicit threshold is imposed to separate low-NOx and high-NOx regimes. Pathway contributions are determined dynamically by competition between RO_2 reacting with NO and RO_2 reacting with HO_2. ~~To avoid double counting, the OH-initiated isoprene oxidation pathway in the VBS scheme is removed (see Sect. 2.1.1).~~ To avoid double counting between the default lumped VBS representation of ISOA and the explicitly represented epoxide-derived ISOA pathways, the OH-initiated isoprene oxidation pathway in the VBS scheme is removed (see Sect. 2.1.1). This treatment focuses the updated mechanism on epoxide-derived ISOA formation, although potential non-epoxide isoprene SOA contributions originally included implicitly in the VBS scheme may not be explicitly resolved.

The reactive uptake parameterization and condensed-phase reaction constants used in this study were adopted from the IEPOX reactive uptake framework of Jo et al. (2019, 2021). Due to limited laboratory constraints on the multiphase kinetics of HMML and MAE (Nguyen et al., 2015), HMML and MAE are treated as IEPOX-like epoxide precursors in the current implementation. This treatment is consistent with previous modeling practice. For example, Pye et al. (2013) treated HMML like MAE in terms of heterogeneous uptake and assumed the particle-phase reaction rate constants of MAE to be the same as those of IEPOX due to the lack of kinetic data. Zhang et al. (2022) also noted that most HMML-related reaction parameters in models are commonly assumed to be the same as those for IEPOX. Following these studies, HMML and MAE are assigned the same solubility, diffusivity, and condensed-phase reaction constants as IEPOX in our implementation. Although a recent field-based study has estimated effective uptake parameters for IEPOX and lumped HMML/MAE, these constraints are not directly applicable here because they do not provide a complete set of standalone, compound-specific solubility, diffusivity, and branch-resolved condensed-phase reaction constants for HMML and MAE (Zhu et al., 2025). **As a result**, this IEPOX-like treatment introduces uncertainty in the absolute uptake rates of HMML and MAE and may affect the modeled quantitative partitioning between high-NOx and low-NOx ISOA formation pathways.~~Following Jo et al. (2019, 2021), this study implements the heterogeneous uptake of IEPOX (Jo et al., 2019, 2021). Due to limited laboratory constraints on multiphase HMML kinetics, and consistent with previous modeling studies, HMML is represented using the same parameterization as IEPOX (Pye et al., 2013; Zhang et al., 2022). In our implementation, this assumption is further extended to MAE, following earlier modeling practice adopted under limited kinetic constraints (Birdsall et al., 2014; Hu et~~

~~al., 2025), and both HMML and MAE are assigned the same solubility and diffusivity values as IEPOX.~~ This study utilizes the Model for Simulating Aerosol Interactions and Chemistry (MOSAIC) aerosol module (Jo et al., 2019, 2021; Zaveri et al., 2008, 2021) to calculate the dynamic partitioning of H_2SO_4, HNO_3, HCl, and NH_3 across different modes and the associated particle-phase thermodynamics. Aerosol pH for each mode is calculated online using MOSAIC, as integrated into CESM by Zaveri et al. (2021) and Lu et al. (2021) (Lu et al., 2021; Zaveri et al., 2021). Additionally, following Jo et al. (2019), we used the modified version of MOSAIC, which calculates submicron (aitken and accumulation modes) aerosol pH, excluding sea salt (Jo et al., 2019). Subsequently, following the resistor model equation of Gaston et al. (2014), this study calculates the reactive uptake coefficient γ for IEPOX, HMML, and MAE (Gaston et al., 2014). The governing expression is:

$$\frac{1}{\gamma} = \frac{\omega R_p}{4D_{gas}} + \frac{1}{\alpha} + \frac{\omega R_p}{4RTH_{org}D_{org}(q_{org}F-1)}, \quad (1)$$

where γ represents the reactive uptake coefficient, ω is the mean molecular speed of epoxides (m s^{-1}), R_p is the particle radius (m), D_{gas} is the gas-phase diffusion coefficient of epoxides (10^{-5} m^2 s^{-1}), α is the mass accommodation coefficient (0.1), R is the universal gas constant (8.2057 x 10^{-2} L atm mol^{-1} K^{-1}), T is temperature (K), H_{org} is the Henry's law coefficient in the organic layer (2 x 10^6 M atm^{-1}), and D_{org} is the diffusion coefficient of epoxides in the organic layer. The term F is calculated as:

$$F = \frac{coth(q_{org})+h(q_{aq},q^*_{org})}{1+coth(q_{org})h(q_{aq},q^*_{org})}, \quad (2)$$

where the function $h(q_{aq}, q^*_{org})$ is given by:

$$h(q_{aq}, q^*_{org}) = -\tanh(q^*_{org}) \frac{\frac{H_{aq}D_{aq}}{H_{org}D_{org}}(q_{aq}\coth(q_{aq})-1)-(q^*_{org}\coth(q^*_{org})-1)}{\frac{H_{aq}D_{aq}}{H_{org}D_{org}}(q_{aq}\coth(q_{aq})-1)-(q^*_{org}\tanh(q^*_{org})-1)}, \quad (3)$$

here, H_{aq} is the Henry's law coefficient in the aqueous core (1.7 x 10^7 M atm^{-1}), and D_{aq} is the diffusion coefficient of epoxides in the aqueous core (10^{-9} m^2 s^{-1}). The variables q_{org}, q_{aq}, and q^*_{org} are defined as:

$$q_{org} = R_p\sqrt{\frac{k_{org}}{D_{org}}}, \quad (4)$$

$$q_{aq} = R_c\sqrt{\frac{k_{aq,total}}{D_{aq}}}, \quad (5)$$

$$q^*_{org} = \frac{R_C}{R_p}q_{org}, \quad (6)$$

where R_C is the inorganic aqueous core radius (m), k_{org} is the pseudo-first-order reaction rate constant of epoxides in the organic shell (s^{-1}), and $k_{aq,total}$ is the total pseudo-first-order aqueous-phase reaction rate constant (s^{-1}), calculated as the

sum of all particle-phase reaction channels that consume each precursor~~Where R_e is the inorganic aqueous core radius (m). k_{aq} is the first-order reaction rate constant in the aqueous phase (s^{-1}), calculated as follows~~:

~~$$k_{aq} = (k_{H^+}[H^+]) + (k_{nuc}[nuc]a_{H^+}) + k_{ga}[ga] \quad (7)$$~~

~~Here, k_{H^+} is the rate constant for the acid-catalyzed ring opening pathway (0.036 M^{-1} s^{-1}), $[H^+]$ is the proton concentration (M), and a_{H^+} denotes proton activity. k_{nuc} represents the reaction rate constant due to the presence of specific nucleophiles (sulfate and nitrate) (2 x 10^{-4} M^{-1} s^{-1}), [nuc] is the concentration of nucleophiles (M). k_{ga} is the reaction rate constant due to the presence of general acids (bisulfate) (7.3 x 10^{-4} M^{-1} s^{-1}), and [ga] is the general acid concentration (M). This study follows the approach of Jo et al. (2021), where the reactivity of epoxides in the organic phase was parameterized with the same reaction rate constant as in the aqueous phase (k_{org}=k_{aq}). Furthermore, considering the strong sensitivity of D_{org} to relative humidity (RH) in the atmosphere, this study accounts for the RH dependence of D_{org}, as described in Table S3 of Zhang et al. (2018) (Zhang et al., 2018).~~

$$k_{aq,total} = k_{H^+}[H^+] + k_{nuc}([SO_4^{2-}] + [NO_3^-])[H^+] + k_{HSO_4^-}[HSO_4^-] \quad (7)$$

The first term represents the acid-catalyzed ring-opening followed by nucleophilic addition of aerosol liquid water, leading to H_2O-mediated nucleophilic addition products. Here, k_{H^+} is the corresponding effective H_2O-mediated nucleophilic addition rate constant (0.036 M^{-1} s^{-1}), with aerosol liquid water treated as the solvent and included implicitly, and $[H^+]$ is the proton concentration (M). The second term represents acid-catalyzed ring opening followed by nucleophilic addition of sulfate and nitrate ions, leading to organosulfates and organonitrates. Here, k_{nuc} is the third-order rate constant for sulfate- and nitrate-addition reactions (2 x 10^{-4} M^{-2} s^{-1}), and $([SO_4^{2-}] + [NO_3^-])$ is the concentration of sulfate and nitrate ions (M). The third term represents concerted protonation and nucleophilic addition by bisulfate, leading to organosulfates. $k_{HSO_4^-}$ is the reaction rate constant due to the presence of bisulfate (7.3 x 10^{-4} M^{-1} s^{-1}), and $[HSO_4^-]$ is the bisulfate concentration (M).

For each precursor considered here, including IEPOX, HMML, and MAE, $k_{aq,total}$ is used to calculate the reactive uptake coefficient and the total uptake flux. The resulting particle-phase ISOA production is then distributed into the H_2O-mediated nucleophilic addition and inorganic-nucleophile addition product classes according to the relative contribution of each reaction channel to $k_{aq,total}$. The H_2O-mediated nucleophilic addition class is represented by the $k_{H^+}[H^+]$ channel, whereas the inorganic-nucleophile addition class combines the sulfate-, nitrate-, and bisulfate-assisted channels, which are collectively represented by $k_{nuc}([SO_4^{2-}] + [NO_3^-])[H^+] + k_{HSO_4^-}[HSO_4^-]$. The corresponding branching ratios for the two product classes are defined as BR_{H_2O} and $BR_{SO_4/NO_3/HSO_4}$, respectively:

$$BR_{H_2O} = \frac{k_{aq,H_2O}}{k_{aq,total}} = \frac{k_{H^+}[H^+]}{k_{aq,total}} \quad (8)$$

$$BR_{SO_4/NO_3/HSO_4} = \frac{k_{aq,SO_4/NO_3/HSO_4}}{k_{aq,total}} = \frac{k_{nuc}([SO_4^{2-}]+[NO_3^-])[H^+]+k_{HSO_4^-}[HSO_4^-]}{k_{aq,total}} \quad (9)$$

This relative-rate branching treatment follows the approach of Budisulistiorini et al. (2017), in which SOA_{IEPOX} speciation between tetrols and organosulfates was determined from the relative rates of precursor conversion to these products. This study follows the approach of Jo et al. (2021), where the reactivity of epoxides in the organic shell was parameterized with the same reaction rate constant as in the aqueous phase ($k_{org} = k_{aq,total}$). This treatment follows the Jo et al. (2019, 2021) core–shell framework and represents a simplifying assumption, because phase separation, organic-shell viscosity, and differences in acidity between the inorganic core and organic shell may alter epoxide diffusion and reactivity (Schmedding et al., 2020; Farrell et al., 2025). Furthermore, considering the strong sensitivity of D_{org} to relative humidity (RH) in the atmosphere, this study accounts for the RH dependence of D_{org}, as described in Table S3 of Zhang et al. (2018) (Zhang et al., 2018).

As illustrated in Fig. 1, the uptake-derived ISOA product classes are mapped to four model species. ISOA formed from the heterogeneous uptake of IEPOX is divided into two product classes: 2-MT (AIETET), produced through the H_2O-mediated nucleophilic addition channel, and organosulfate/organonitrate products (AIEOSN), produced through the inorganic-nucleophile addition channel. Similarly, ISOA formed from HMML and MAE is divided into 2-MG (AHMGA), produced through the H_2O-mediated nucleophilic addition channel, and organosulfate/organonitrate products (AHMOSN), produced through the inorganic-nucleophile addition channel.~~In this study, the SOA formed from the heterogeneous reactions of IEPOX includes 2-MT (AIETET) and organosulfates/organonitrates (AIEOSN), which result from nucleophilic addition with aerosol liquid water and sulfate/nitrate, respectively. Similarly, SOA from HMML and MAE consists of 2-MG (AHMGA) and organosulfates/organonitrates (AHMOSN), both of which are produced through nucleophilic addition involving aerosol liquid water and sulfate/nitrate.~~ The SOA yield from the reactive uptake of IEPOX, HMML, and MAE is assumed to be 100%, and SOA derived from these epoxides is treated as non-volatile in the model. This assumption is in agreement with previous modeling studies (Budisulistiorini et al., 2017; Marais et al., 2016; Schmedding et al., 2019; Stadtler et al., 2018), which are based on field observations indicating that SOA from these epoxides in the atmosphere exhibits very low volatility (Hu et al., 2016; Riva et al., 2019). Once SOA from IEPOX, HMML, and MAE is formed, no further oxidation occurs in the model, consistent with previous studies (Budisulistiorini et al., 2017; Marais et al., 2016; Schmedding et al., 2019).

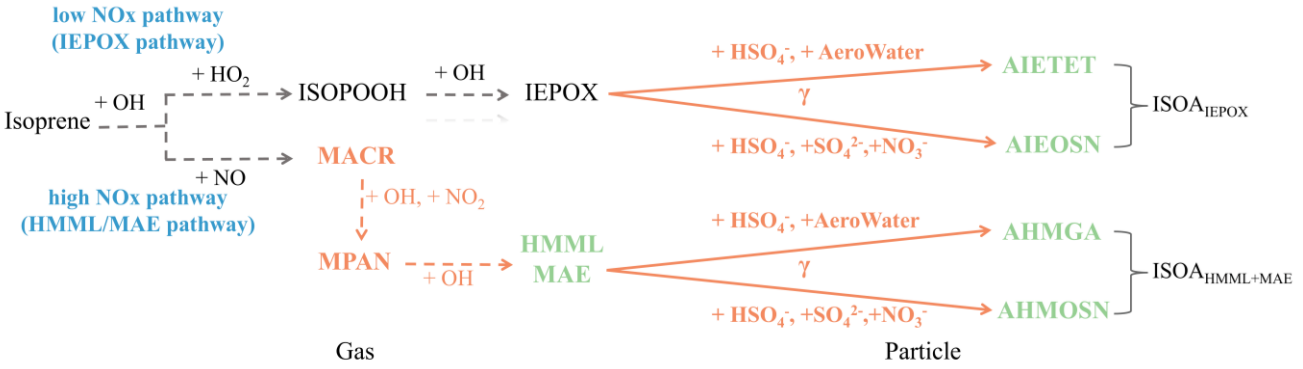

Figure 1: Schematic of the explicit isoprene-derived secondary organic aerosol (ISOA) formation mechanism implemented in CAM6-Chem in this study. Dashed arrows indicate gas-phase reactions, whereas solid arrows indicate particle-phase heterogeneous uptake and product-formation reactions. Species explicitly represented as updated ISOA precursors or product classes in this mechanism are shown in green, and the explicitly represented ISOA formation pathways are shown in orange. AeroWater denotes aerosol liquid water. AIETET denotes IEPOX-derived 2-methyltetrols, AIEOSN denotes IEPOX-derived organosulfate/organonitrate products, AHMGA denotes HMML/MAE-derived 2-methylglyceric acid, and AHMOSN denotes HMML/MAE-derived organosulfate/organonitrate products.

2.2 Model experiments and observational data

This study simulates the years 2000, 2006, 2012, 2016, and 2019 at a horizontal resolution of 0.95° (latitude) × 1.25° (longitude). The vertical grid comprises 32 layers with a model top of around 40 km. For each simulated year, a 3-month spin-up is applied to minimize the influence of initial conditions, and a 50 h relaxation (nudging) timescale is used throughout the simulation.

This study uses ground-based observations reported by Ding et al. (2016) (Ding et al., 2016). The record spans October 2012 to September 2013 and provides annual and seasonal mass concentrations of two ISOA tracers, AIETET and AHMGA. The dataset comprises twelve sites, including five urban, three suburban, and four rural locations, and provides the geographic coordinates for each site. In total, 294 sets of field samples were compiled across the four seasons and summarized by site and by season for both tracers, enabling comparison with the model on consistent temporal and spatial scales. In addition, we used observations reported by Zhang et al. (2022), who conducted a 1-year measurement campaign from October 2013 to November 2014 at three urban sites from northern to southern China, namely Beijing, Hefei, and Kunming (Zhang et al., 2022). This dataset reports paired ISOA products formed through the IEPOX and HMML pathways, and provides site-resolved annual-average concentrations for key species, which are useful for evaluating the simulated ISOA composition and pathway partitioning over urban China. In addition, we used ground-based observational compilations assembled by Miao et al. (2021) and Chen et al. (2024a). These compilations summarize site-mean surface mass concentrations of OA, POA, and SOA across China for 2013–2019, together with the corresponding site location (Chen et al., 2024a; Miao et al., 2021). After selecting records within our study period and removing duplicates, a total of 39 measurements were retained for model evaluation.

3. Results and Discussions

3.1 Evaluation of model performance

This section first evaluates the simulation results based on observational data, and then summarizes the overall characteristics of the simulated ISOA, including concentration levels, major subclasses, and spatial distribution.

By comparing the simulated results with ground-based observations, we evaluated the performance of the improved CAM6-Chem (Fig. 2). For all NMB calculations in this section, model outputs were sampled at the corresponding observational site locations and averaged over the same observational periods before calculating the model–observation differences. The paired model and observational values from different sites and time periods were then combined across all paired samples to calculate the NMB, thereby accounting for the site-specific locations and different temporal coverage of the observational datasets. Overall, the mechanism-updated model can more comprehensively capture the concentrations of key ISOA subspecies and better reproduce their relative contributions (Fig. 2(c)). Additionally, it alleviates the systematic underestimation of OA and SOA in the earlier CAM6-Chem configuration~~pre-update version~~ (Zhang et al., 2025). We evaluated~~validated~~ the simulated AIETET and AHMGA against ground-based observations from Ding et al. (2016) (Fig. 2(a)). The updated simulation generally captures the concentration ranges and variability of these two subspecies, but still shows an overall positive bias. Based on monthly means in log space, the normalized mean biases (NMB) are 61.4% for AIETET and 89.1% for AHMGA, with corresponding Pearson correlation coefficients (r) values of 0.56 and 0.29, respectively.~~Based on monthly means in log space, the normalized mean biases (NMB) are 47.4% for AIETET and 81.6% for AHMGA, with corresponding R^2 values of 0.50 and 0.42, respectively.~~ Several factors may contribute to these positive biases. First, missing or simplified competing loss pathways may cause an over-allocation of epoxide precursors to the explicitly represented ISOA product. For example, a fraction of IEPOX-derived products in the real atmosphere may be diverted to C5-alkene triols or other particle-phase products that are not explicitly represented here, thereby reducing the effective yield of AIETET (Pye et al., 2013).~~This bias may reflect remaining uncertainties in the representation of precursor loss pathways and multiphase processing in the mechanism. For example, a fraction of precursors in the real atmosphere may be diverted into alternative reaction channels and further converted to C5-alkene triols, thereby reducing the effective yields feeding the corresponding ISOA subspecies (Pye et al., 2013).~~ In addition, previous studies have shown that AIETET and AHMGA are sensitive to factors such as pathway branching, mass transfer, reaction kinetics, and aerosol phase state. For example, uncertainties in the relative rates of water addition versus organosulfate formation can affect the predicted product distribution between 2-MT and organosulfate products (Budisulistiorini et al., 2017). Similarly, assumptions related to aerosol phase state, organic-shell viscosity, and phase separation can influence IEPOX reactive uptake and may affect the simulated abundance of IEPOX-derived tracers (Zhang et al., 2019; Chen et al., 2024). In particular, the current core–shell uptake treatment assumes the same reaction rate coefficient in the organic shell and aqueous core. If phase separation and viscous organic coatings impose stronger diffusion limitations than represented here, effective epoxide uptake may be

reduced in the real atmosphere, and the model may overestimate ISOA formation, especially under conditions with high organic coatings or strong phase separation. For AHMGA, uncertainties in the multiphase uptake and reaction parameters of HMML/MAE may also contribute to the model bias, because compound-specific constraints for these high-NOx epoxides remain limited (Zhang et al., 2022; Zhu et al., 2025). Accordingly, positive biases of several tens of percent have also been reported in earlier modeling studies. For instance, Fahey et al. (2017) reported that, in a regional evaluation using the Community Multiscale Air Quality (CMAQ) model, the NMB of AHMGA reached 78.6% under an updated scheme (Fahey et al., 2017), whereas Chen et al. (2024) found a pronounced overestimation of AIETET in a baseline configuration (NMB = 58%) in their evaluation of IEPOX multiphase parameterization (Chen et al., 2024b). Therefore, the magnitude of the overestimation in this study is comparable to that reported previously, although the exact sources of bias may differ across models and configurations. It further suggests that incorporating a more complete set of competitive loss processes and additional constraints on multiphase chemistry may help reduce subspecies-level biases in future work.

At the bulk OA and SOA levels, we further evaluated model performance against observations from Miao et al. (2021) and Chen et al. (2024a) (Chen et al., 2024a; Miao et al., 2021) by comparing the simulated results from the earlier CAM6-Chem configuration described by Zhang et al. (2025) with those from the CAM6-Chem configuration using the explicit ISOA representation adopted in this study (Fig. 2(b)).~~At the bulk OA and SOA levels, we further evaluated model performance against observations from Miao et al. (2021) and Chen et al. (2024a) (Chen et al., 2024a; Miao et al., 2021) by comparing the pre-update version (Zhang et al., 2025) with the updated version (Fig. 2(b)).~~ The results show that the mechanism update substantially reduces the underestimation of SOA, with the NMB improving from −76.7% to −~~50.0~~51.6%~~, mainly owing to improved ISOA simulation~~. This improvement reflects the enhanced representation of ISOA formation introduced in this study, since other SOA formation pathways were not modified in the updated mechanism. The underestimation of total OA is also alleviated, with the NMB improving from −47.0% to −~~24.5~~25.7%. Beyond this bulk evaluation, we further assessed model performance at the molecular-species level using ground-based measurements of ISOA tracers from Beijing, Hefei, and Kunming (Zhang et al., 2022) (Fig. 2(c)). The comparison shows that the updated mechanism can reproduce the major observed ISOA species and yields a more realistic compositional distribution than the pre-update version. In particular, the simulation using this explicit ISOA representation reproduces the dominant contribution of AIETET and the relatively small contributions of inorganic-nucleophile addition class products, including AIEOSN and AHMOSN. This result indicates that the product-speciation treatment captures the observed dominance of H_2O-mediated nucleophilic addition products in the available molecular tracer composition, which is also consistent with previous field observations showing relatively small inorganic-nucleophile addition products contributions (He et al., 2018). Nevertheless, residual discrepancies in individual species fractions may still reflect uncertainties in the reactive uptake parameterization, possible missing transformation or loss processes, and the representation of the heterogeneous reaction medium, including the effective abundance and accessibility of different inorganic nucleophiles.~~In particular, the relative contributions of ISOA subspecies associated with the newly introduced reaction pathways are better captured, indicating that the mechanism update improves not only the total~~

~~ISOA abundance but also its chemical speciation. Although some discrepancies in the fractional contributions of individual species remain, the updated simulation captures the observed multi-component nature of ambient ISOA much more successfully than the previous version.~~ This improvement is important because it demonstrates that the added reaction pathways are chemically meaningful and enhance the model's capability to reproduce both the magnitude and composition of ambient ISOA, providing a more robust modeling foundation for the subsequent quantitative attribution of ISOA changes and their driving factors.

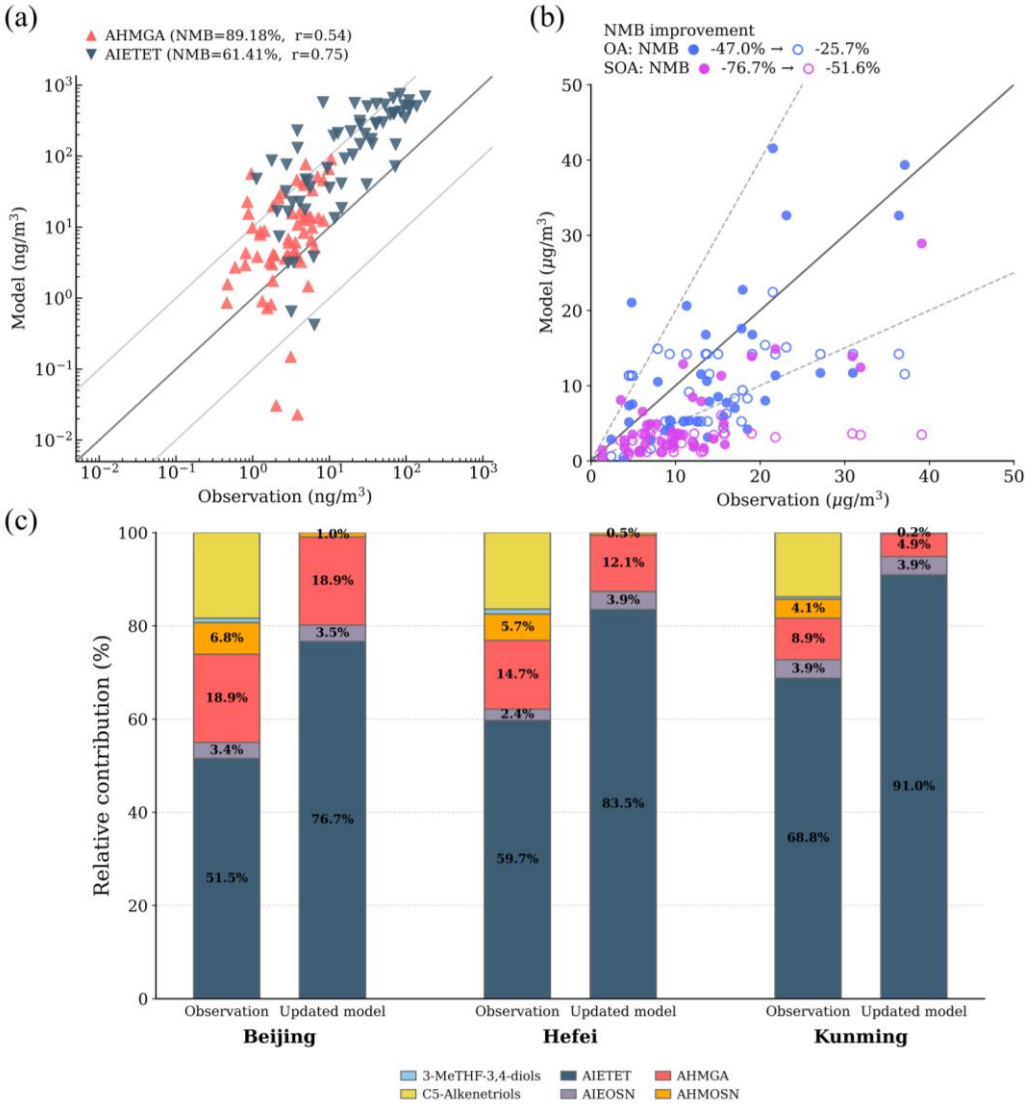

Figure 2: (a) Evaluation of simulated 2-methyltetrols (AIETET) and 2-methylglyceric acid (AHMGA) concentrations against ground-based observations from Ding et al. (2016) (ng m^{-3}). Statistical metrics were calculated using monthly means in log space. The dark gray solid line denotes the 1:1 line, and the light gray solid lines denote the factor-of-10 range. (b) Evaluation of

simulated organic aerosol (OA) and secondary organic aerosol (SOA) concentrations before and after the mechanism update against ground-based observations compiled from Miao et al. (2021) and Chen et al. (2024a) (μg m^{-3}). Filled circles represent simulations before the update, while open circles represent simulations after the update. Blue and magenta markers denote OA and SOA, respectively. The inset annotation summarizes the changes in normalized mean bias (NMB) from the original to the updated simulation. The dark gray solid line denotes the 1:1 line, and the light gray dashed lines denote the factor-of-two range. (c) Comparison of ISOA product composition between ground-based observations adapted from Zhang et al. (2022) and the updated model simulation in this study. The grouped stacked bars show the relative contribution of each ISOA product to total measured or simulated ISOA at Beijing, Hefei, and Kunming. For each city, the left bar represents the observed composition and the right bar represents the updated model.

3.2 General characteristics of ISOA and contribution from new chemical pathways

The simulations show pronounced regional contrasts in the spatial distribution of ISOA over China (Fig. 3(a)). Total ISOA forms a major hotspot in Southwest China (>1000 ng m^{-3}), remains relatively high in Southeastern China, and is generally lower over North China and Northwestern China. In terms of composition, AIETET is the dominant subspecies and accounts for the largest national fraction (~~49.6~~88.9%). ~~AIEOSN~~AHMGA is the second-largest contributor (~~44.0~~6.9%). The spatial patterns of these two subspecies are broadly consistent with the hotspot of total ISOA (Fig. S1). In contrast, ~~AHMGA~~ AIEOSN (~~3.4~~3.9%) and AHMOSN (~~3.0~~0.3%) contribute less to the national burden on average. They are more pronounced in typical high-emission regions in Eastern China. This enhancement is especially evident over major urban and industrial clusters such as the North China Plain, the Yangtze River Delta, and the Pearl River Delta (Fig. 3(c)). In these NOx-rich regions, the relative contributions of AHMGA and AHMOSN increase markedly. Together they account for approximately ~~15–20~~17-21% of the total ISOA. ~~The three newly added subspecies in this study include AIETET, AHMGA, and AHMOSN. Their contributions to total ISOA are non-negligible. They contribute about 56% on the national average (Fig. 3(b)) and also represent substantial fractions across different region types (Fig. 3(c)).~~ These results indicate that the explicit ISOA representation adopted in this study enables a more comprehensive characterization of ISOA composition and concentration levels by resolving uptake-derived ISOA into different product classes.~~These results indicate that improving the multiphase chemistry enables a more comprehensive characterization of ISOA composition and concentration levels.~~ It is also noteworthy that the concentration differences of AHMGA and AHMOSN between polluted regions and the southwestern hotspot are smaller than those of the low-NOx pathway products (Fig. S1). This feature indicates a relatively more spatially distributed pattern for these high-NOx pathway products. Overall, the subspecies collectively characterize the spatial heterogeneity of ISOA. Low-NOx pathway components dominate the national burden and define the primary hotspot. High-NOx pathway components contribute less to the national average burden, but their relative contributions are more evident over eastern urban and industrial regions (Fig. 3(c)).

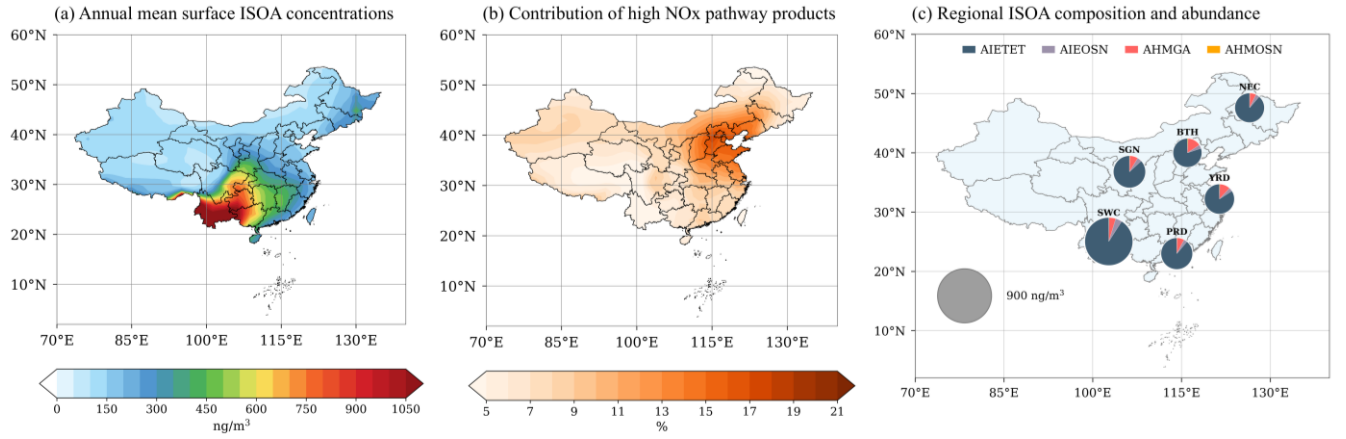

Figure 3: (a) Annual mean surface concentrations of isoprene-derived secondary organic aerosol (ISOA) over China, averaged over the five simulation years (2000, 2006, 2012, 2016, and 2019) (unit: ng m^{-3}). (b) Spatial distribution of the contribution of high-NOx pathway products, including 2-methylglyceric acid (AHMGA) and organosulfate/organonitrate products from the high-NOx pathway (AHMOSN), to annual mean total ISOA over China, averaged over the five simulation years (unit: %). (c) Composition of surface ISOA subspecies in six regions of China, including Southwest China (SWC), the Beijing–Tianjin–Hebei region (BTH), the Yangtze River Delta (YRD), the Pearl River Delta (PRD), the Shaanxi–Gansu–Ningxia region (SGN), and Northeast China (NEC), based on annual mean concentrations averaged over the five simulation years. Pie charts show the fractional contributions of individual ISOA subspecies, and the circle size represents the corresponding surface ISOA concentration (unit: ng m^{-3}).

In addition to the pronounced spatial heterogeneity, ISOA also shows strong seasonal variability (Fig. 4). Based on the 5-year monthly means, surface ISOA increases markedly during the warm season and reaches a maximum in summer. Summer ISOA concentrations are approximately 3 to 5 times higher than those in winter (Fig. 4(a)). The compositional information in Fig. 4(a) further shows that this warm-season enhancement is mainly associated with $ISOA_{IEPOX}$, especially AIETET. AIEOSN and $ISOA_{HMML+MAE}$ remain smaller components of the national mean ISOA, although they also increase during the warm season. This indicates that the seasonal cycle of total ISOA is primarily driven by AIETET, the H_2O-mediated nucleophilic-addition product of IEPOX, while inorganic-nucleophile-addition products of IEPOX and $ISOA_{HMML+MAE}$ provide secondary contributions to the overall seasonal variation. Biogenic isoprene emissions exhibit a similar seasonal cycle. They increase rapidly from spring and peak in summer, which is generally consistent with the timing of the ISOA maximum (Fig. 4(a)). The standardized seasonal cycle further shows that the standardized OH signal also peaks in summer, indicating that enhanced precursor supply and oxidation capacity jointly support the summer ISOA maximum (Fig. 4(b)). However, the standardized sulfate and aerosol liquid water show different seasonal patterns from total ISOA. The standardized sulfate and aerosol liquid water anomalies are positive in winter and become negative in summer, while the standardized aerosol pH anomaly shows positive anomalies in late spring and early summer (Fig. 4(b)). Therefore, the summer ISOA maximum occurs even when sulfate and aerosol liquid water are relatively low, suggesting that the strong increases in isoprene emissions and OH oxidation capacity outweigh the less favorable multiphase conditions during summer. The early warm-season ISOA enhancement from April to May further illustrates this combined-control behavior, but with a different balance among the controlling factors. It occurs before the annual maxima of isoprene emissions and during the

rising phase of the standardized seasonal OH signal, but at a time when biogenic isoprene emissions have already increased substantially from spring, OH oxidation capacity is strengthening, and the multiphase reaction environment has not yet reached its least favorable summer state. Thus, the May enhancement likely reflects the combined influence of increasing precursor supply, enhanced oxidation, and still favorable multiphase conditions, rather than the dominance of a single factor. Overall, these features indicate that the seasonal cycle of total ISOA cannot be explained by one controlling factor alone, but instead reflects the combined effects of emission strength, oxidation intensity, and multiphase chemical conditions. ~~Biogenic isoprene emissions exhibit a similar seasonal cycle. They increase rapidly from spring and peak in summer, which is generally consistent with the timing of the ISOA maximum (Fig. 4(a)). The seasonal variation of ISOA reflects the seasonal co-variations in precursor availability and in the chemical and multiphase environment (Fig. 4(b)). The standardized seasonal cycle indicates that the OH anomaly peaks in summer, which coincides with the period of elevated ISOA (Fig. 4(b)). In contrast, the standardized sulfate and aerosol liquid water anomalies are positive in winter and negative in summer. The standardized aerosol pH anomaly also varies substantially through the year, with positive anomalies in late spring and early summer (Fig. 4(b)). Therefore, even when the standardized anomalies of sulfate, aerosol liquid water, and aerosol pH are not all maximized in summer, the coincident summer peaks in isoprene emissions and OH concentrations together lead to the highest ISOA concentrations in summer. This further indicates that the seasonal cycle of total ISOA cannot be explained by a single controlling factor and instead reflects the combined effects of emission strength, oxidation intensity, and multiphase chemical conditions.~~

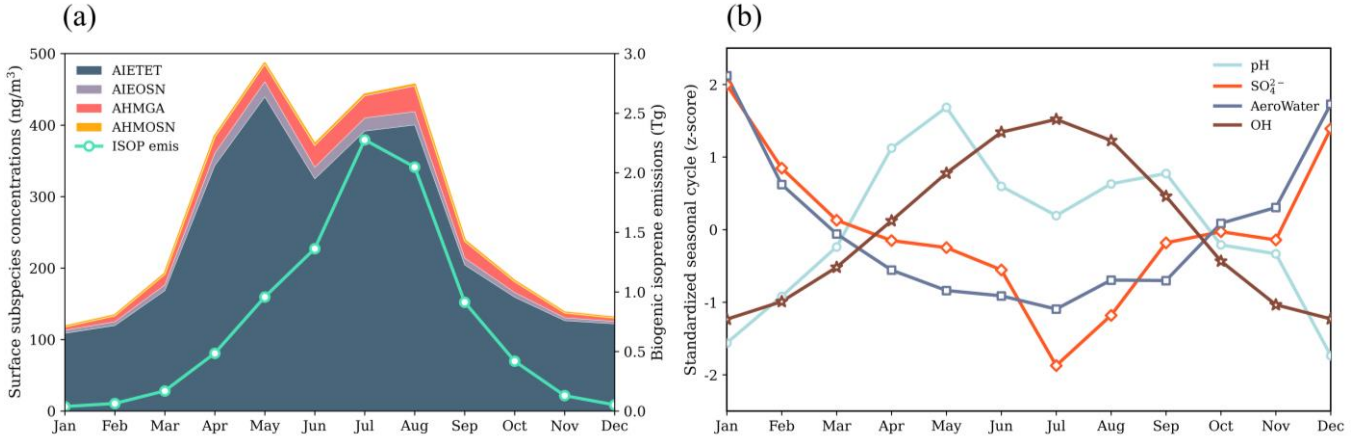

Figure 4: (a) Monthly variations of surface isoprene-derived secondary organic aerosol (ISOA) subspecies (left y axis; unit: ng m^{-3}) and biogenic isoprene emissions (ISOP emis; right y axis; unit: Tg) in China, based on the climatological monthly means averaged over the five simulation years (2000, 2006, 2012, 2016, and 2019). (b) Standardized monthly variations of background chemical and aerosol variables relevant to ISOA formation, including surface aerosol pH, surface sulfate (SO_4^{2-}) concentrations, surface aerosol liquid water (AeroWater) concentrations, and surface hydroxyl radical (OH) concentrations in China, based on the climatological monthly means averaged over the five simulation years.

ISOA formation is strongly influenced by the NOx background, so competition exists between the IEPOX pathway and the MAE/HMML pathway. Overall, the MAE/HMML pathway contributes less to ISOA than the IEPOX pathway, but its relative importance varies across regions and seasons.

We use ratio-based metrics to quantify the relative contributions of the two pathways. For the national mean $ISOA_{HMML+MAE}$ (ISOA derived from HMML and MAE)/$ISOA_{IEPOX}$, the annual mean ratio is about 0.07, indicating that the IEPOX pathway dominates at the national scale. A further analysis for densely populated regions such as the Beijing-Tianjin-Hebei region shows a higher ratio that still remains well below 1 (Fig. S7). This indicates that the IEPOX pathway remains the primary source of ISOA even in NOx-rich regions.

The national mean $ISOA_{HMML+MAE}/ISOA_{IEPOX}$ is not constant throughout the year. It becomes relatively higher in late summer and early autumn and reaches its annual maximum in September (Fig. 5(c)). To interpret this feature, we further compare the gas-phase precursors and particle-phase production rates diagnosed from the tagged heterogeneous reactions for~~heterogeneous reaction intensities of~~ the two pathways. The ratio of the gas-phase epoxide precursors HMML + MAE to IEPOX shows only a modest seasonal variation and generally remains within about 0.08 to 0.10 throughout the year (Fig. 5(a)). The ratio of tagged particle-phase ISOA production rates, $P_{HMML+MAE}/P_{IEPOX}$~~, The ratio of heterogeneous reaction rates $K_{het\_HMML+MAE}$ (heterogeneous reaction rates of HMML + MAE)/K_{het_IEPOX} (heterogeneous reaction rates of IEPOX)~~ exhibits a similar seasonal pattern, with an annual mean of about 0.10 to 0.11 (Fig. 5(b)). These results indicate that neither the HMML+MAE-to-IEPOX precursor ratio nor the corresponding tagged particle-phase ISOA production-rate ratio shows a comparably strong increase in September. Therefore, the September peak in the $ISOA_{HMML+MAE}/ISOA_{IEPOX}$ ratio is not primarily driven by an enhanced relative precursor abundance or production rate of the HMML/MAE pathway, but rather by the stronger decrease in $ISOA_{IEPOX}$ relative to $ISOA_{HMML+MAE}$ from August to September, as shown in Fig. 5(c). As a result, the $ISOA_{HMML+MAE}/ISOA_{IEPOX}$ ratio increases from 0.089 in August to 0.114 in September, corresponding to an absolute increase of 0.025 in the dimensionless ratio, or a relative increase of 28.1%, and reaches its annual maximum in September.~~These results indicate that the relative precursor supply and heterogeneous reaction intensity of HMML + MAE compared with IEPOX do not show a comparably strong increase in September. Therefore, the September peak in the ratio is more likely driven by relative changes in product concentrations. Fig. 5(c) shows that the decrease in $ISOA_{IEPOX}$ from August to September is much larger than the decrease in $ISOA_{HMML+MAE}$. As a result, $ISOA_{HMML+MAE}/ISOA_{IEPOX}$ increases markedly and peaks in September.~~ Overall, the MAE/HMML pathway becomes relatively more important in NOx-rich regions and during late summer to early autumn, but the IEPOX pathway still dominates ISOA formation on the national average.

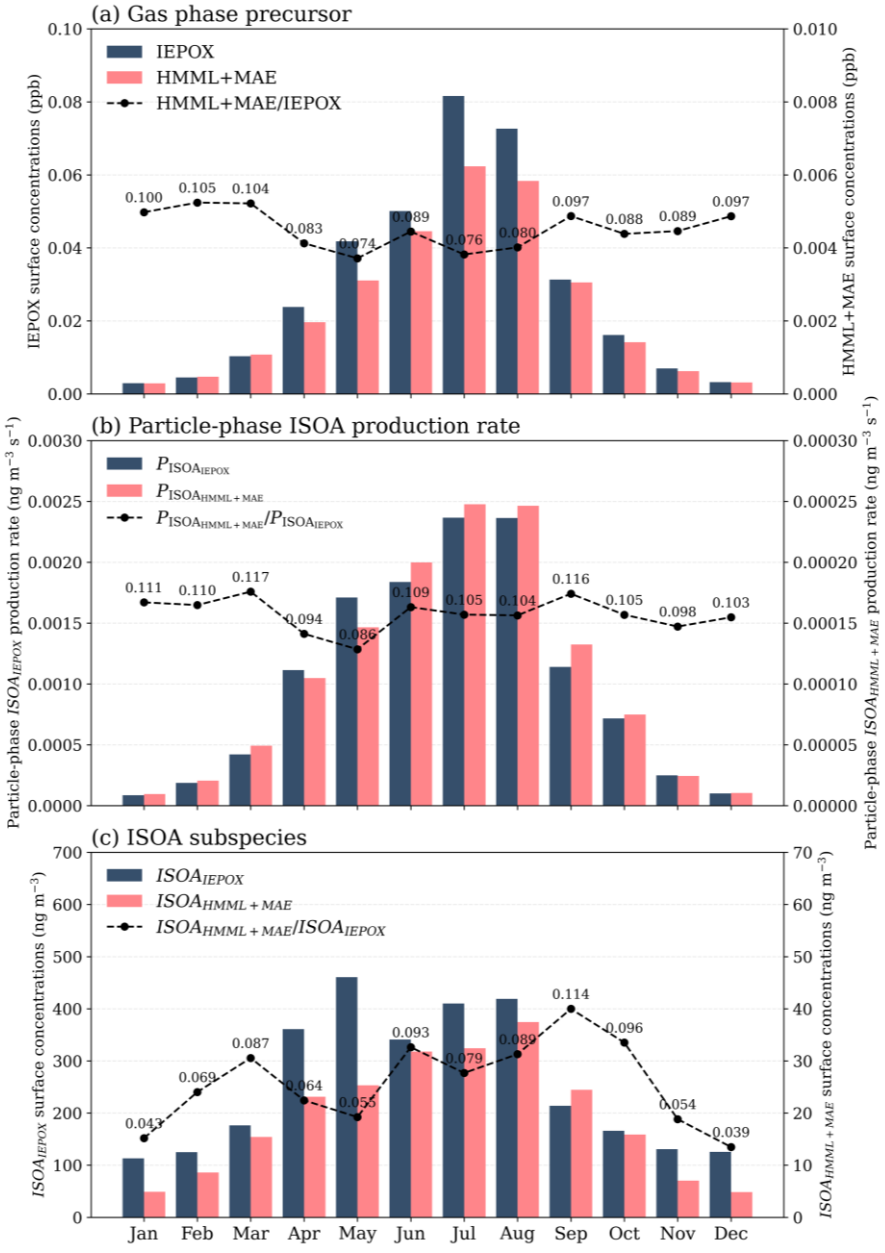

Figure 5: Monthly variations of IEPOX-related and HMML+MAE-related gas-phase precursors, particle-phase production rates, and ISOA concentrations in China, based on the climatological monthly means averaged over the five simulation years (2000, 2006, 2012, 2016, and 2019). (a) Surface concentrations of isoprene epoxydiols (IEPOX; dark-blue bars; left y axis; unit: ppb) and hydroxymethyl-methyl-α-lactone plus methacrylic acid epoxide (HMML + MAE; pink bars; right y axis; unit: ppb). (b) Particle-phase ISOA production rates diagnosed from tagged heterogeneous reactions for the IEPOX pathway ($P_{ISOA_{IEPOX}}$; dark-blue bars; left y axis; unit: ng m^{-3} s^{-1}) and the HMML+MAE pathway ($P_{ISOA_{HMML+MAE}}$; pink bars; right y axis; unit: ng m^{-3} s^{-1}). (c) Surface concentrations of ISOA derived from IEPOX ($ISOA_{IEPOX}$; dark-blue bars; left y axis; unit: ng m^{-3}) and ISOA derived from HMML and MAE ($ISOA_{HMML+MAE}$; pink bars; right y axis; unit: ng m^{-3}). In each panel, the black dashed line denotes the ratio of

the HMML+MAE-related quantity to the corresponding IEPOX-related quantity, with monthly ratio values labeled above the markers.

3.3 Trend and attribution of ISOA

This section first presents the spatial distribution of long-term trends in surface ISOA over China during 2000–2019, along with the corresponding trends in its key controlling factors, and identifies the regions with the most pronounced ISOA changes. It then uses multiple linear regression to diagnose the dominant drivers of simulated ISOA variability. Sulfate and aerosol liquid water can both act as reaction media for heterogeneous processes (Budisulistiorini et al., 2017; Eddingsaas et al., 2010), while proton availability catalyzes the ring-opening of epoxide groups, a key step in ISOA formation (Gaston et al., 2014; Pye et al., 2013). Biogenic isoprene emissions provide the direct gas-phase precursor supply for ISOA formation. Based on these considerations, simulated monthly ISOA concentration was used as the dependent variable, and proton concentration (H^+), sulfate (SO_4^{2-}, μg m^{-3}), biogenic isoprene emissions (ISOP emis, g m^{-2}), and aerosol liquid water (AeroWater, μg m^{-3}) were included as predictors in the regression analysis.

Our nationwide analysis indicates that the long-term evolution of surface ISOA over China is relatively weak in the national mean. Overall, total surface ISOA decreases by 10.23~~=4.62~~ ng m^{-3} per 20 years (-3.67~~=1.28~~% per 20 years) from 2000 to 2019. This net change arises from competing trends among the major ISOA subspecies, with the largest decreases occurring in AIETET, followed by AIEOSN, while concurrent increases in other subspecies partly offset these declines. Over the same period, the key controlling factors also show systematic but contrasting national-scale changes, with biogenic isoprene emissions and anthropogenic NOx emissions increasing by 5.38% and 48.75% per 20 years, respectively, while anthropogenic SO_2 emissions, sulfate, and aerosol liquid water decrease by 75.12%, 43.16%, and 5.54% per 20 years, respectively (Figs. 6 and 7). These changes imply enhanced precursor supply under rising NOx but a weakened heterogeneous reaction medium at the national scale. All trends were derived from linear regressions based on annual data from 2000 to 2019. The weak national-mean trend does not imply spatial uniformity and may instead reflect the cancellation of regionally heterogeneous trends with opposite signs. For this reason, the following analysis focuses on the spatial distribution of ISOA trends and their key driving factors at the regional scale.

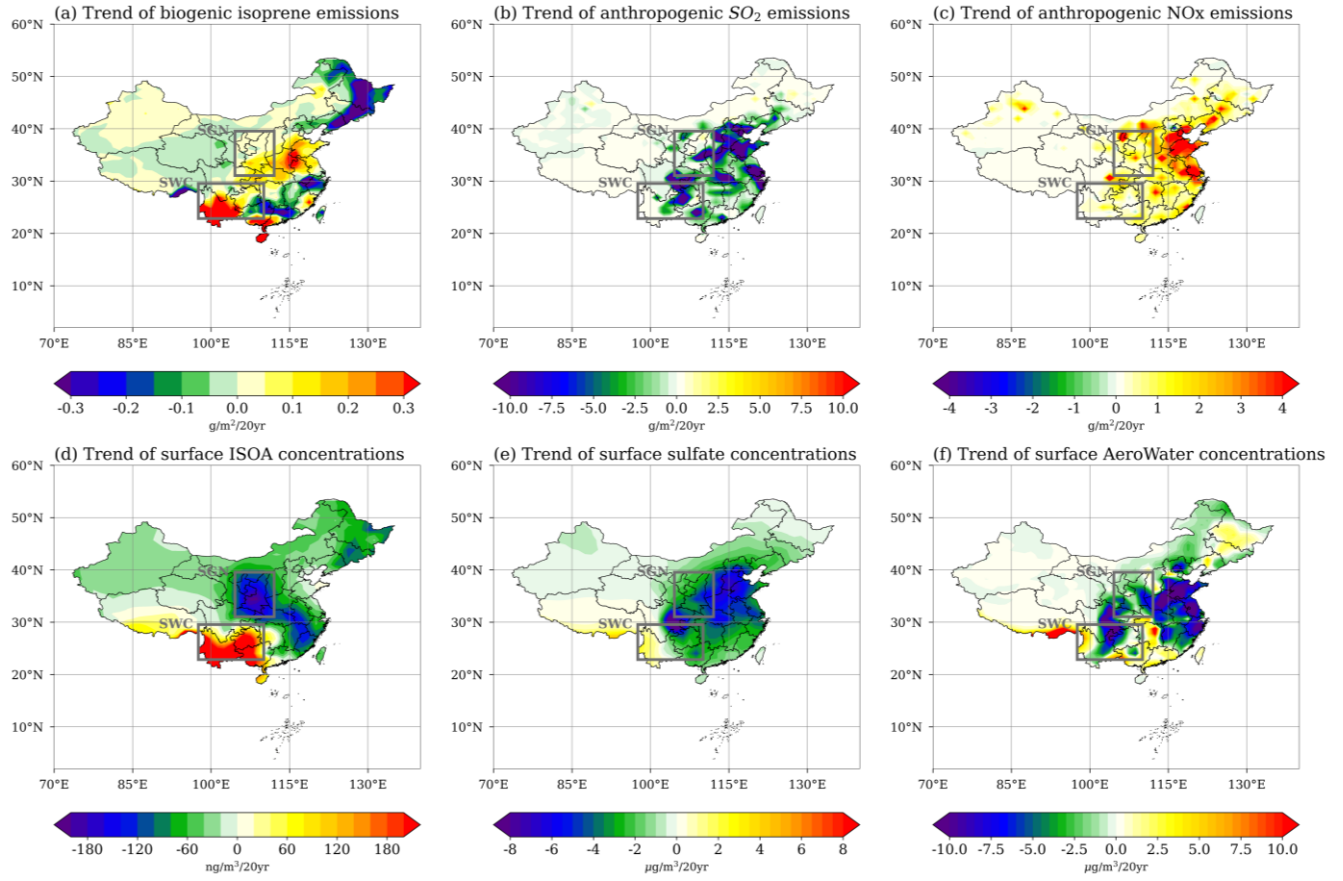

Figure 6: Long-term trends in annual mean surface concentrations of biogenic isoprene emissions (a; unit: g m^{-2} per 20 years), anthropogenic sulfur dioxide (SO_2) emissions (b; unit: g m^{-2} per 20 years), and anthropogenic nitrogen oxides (NOx) emissions (c; unit: g m^{-2} per 20 years), and of surface isoprene-derived secondary organic aerosol (ISOA) concentrations (d; ng m^{-3} per 20 years), surface sulfate concentrations (e; μg m^{-3} per 20 years), and surface aerosol liquid water (AeroWater) concentrations (f; μg m^{-3} per 20 years), in China from 2000 to 2019. The two boxed regions denote Southwest China (SWC) and the Shaanxi–Gansu–Ningxia region (SGN), respectively.

The spatial distribution of long-term trends confirms that the weak national-mean change in surface ISOA is largely caused by strong regional contrasts with opposite signs (Fig. 6(d)). The simulations show that the strongest increasing trend is found in Southwest China (SWC) (Fig. 6(d)), where the annual mean surface ISOA concentration increases significantly by 218.01~~284.27~~ ng m^{-3} per 20 years, corresponding to an increase of 25.27~~25.53~~% per 20 years (Fig. 7(a)). In contrast, the strongest decreasing trend occurs in the Shaanxi–Gansu–Ningxia region (SGN) (Fig. 6(d)), where the annual mean surface ISOA concentration decreases significantly by 142.21~~153.41~~ ng m^{-3} per 20 years, corresponding to a decline of 41.87~~33.88~~% per 20 years (Fig. 7(a)). As these two regions represent the opposite extremes of the national trend pattern, we focus on them in the following analysis to investigate their ISOA changes and the differences in the dominant controlling factors.

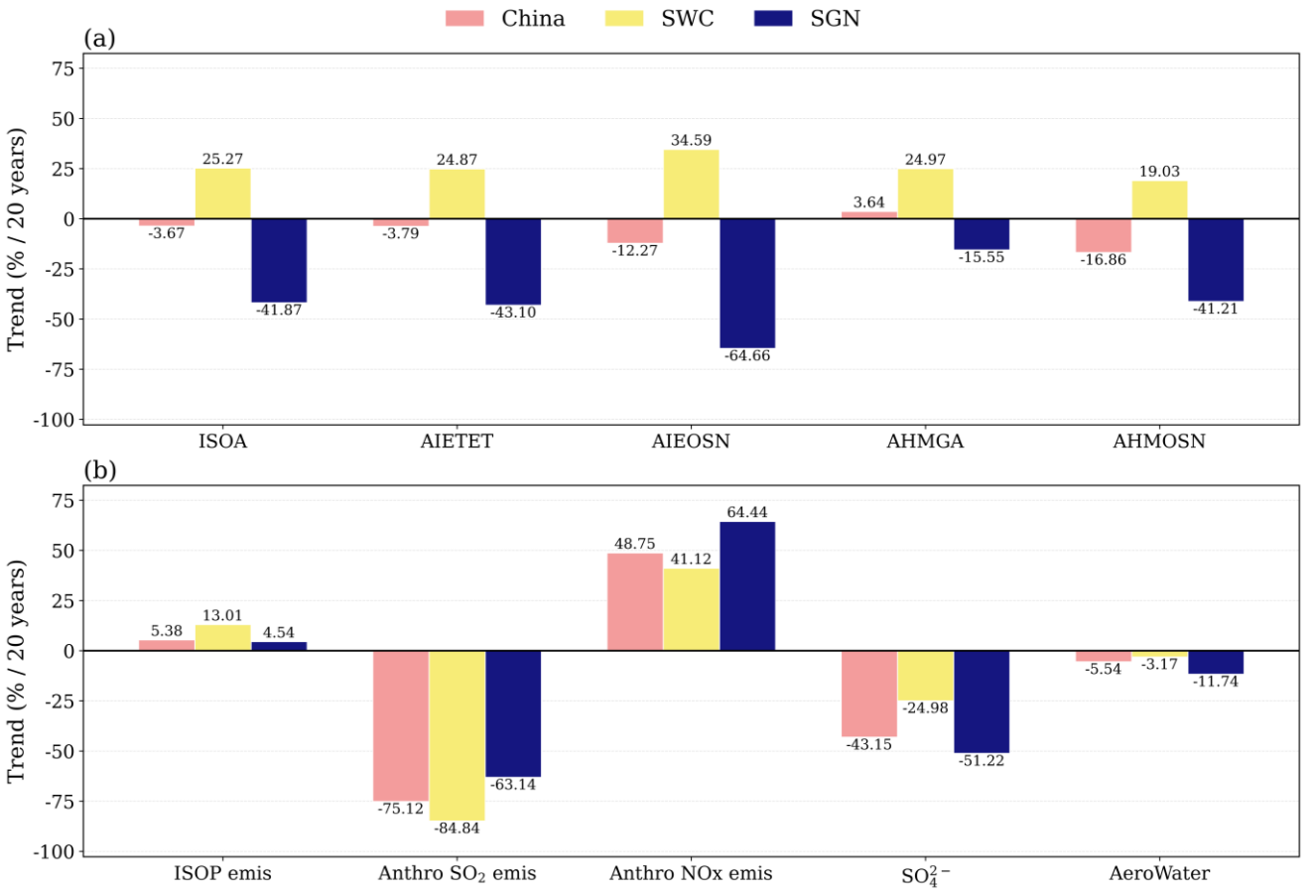

Figure 7: Long-term trends in China (pink bar), Southwest China (SWC; bright yellow bar), and the Shaanxi–Gansu–Ningxia region (SGN; dark blue bar) of (a) surface isoprene-derived secondary organic aerosol (ISOA) and its major subspecies, and (b) biogenic isoprene emissions (ISOP emis), anthropogenic sulfur dioxide (SO_2) emissions (Anthro SO_2 emis), anthropogenic nitrogen oxides (NOx) emissions (Anthro NOx emis), surface sulfate (SO_4^{2-}) concentrations, and surface aerosol liquid water (AeroWater) concentrations. Bars indicate relative trends over 20 years (% / 20 years).

It is noteworthy that, despite broadly similar temporal trends in the key controlling factors over the two regions, surface ISOA exhibits opposite long-term changes. As shown in Fig. 7(a), ISOA increases in SWC but decreases in SGN. The controlling variables generally evolve in similar directions in both regions, although the magnitudes of their changes differ. In the SWC region, surface ISOA exhibits a significant increasing trend (Fig. 6(d)), and the increases among individual ISOA subspecies are broadly comparable, generally on the order of 25% per 20 years (Fig.7(a), S). This enhancement is consistent with signals of regional climate change. Regional temperature increases by 0.24% per 20 years and is accompanied by a pronounced increase in biogenic isoprene emissions of 13.01% per 20 years (Fig. 6(a),7(b)). At the same time, anthropogenic SO_2 emissions decrease by 84.84% per 20 years (Fig. 6(b),7(b)), accompanied by a corresponding decline in sulfate of 24.98% per 20 years (Fig. 6(e),7(b)). Aerosol liquid water also shows a slight decrease of 3.17% per 20 years (Fig. 6(f),7(b)). These results indicate that, in SWC, the increase in isoprene emissions offsets the adverse influence of

declining reaction-medium levels. As a result, surface ISOA still shows a marked increase. In contrast, the substantial decrease in ISOA over SGN mainly results from reductions in products formed through the IEPOX pathway (Fig. 7(a), S4). AIETET and AIEOSN decrease by 127.63~~79.97~~ ng m^{-3} per 20 years and 9.83~~71.10~~ ng m^{-3} per 20 years, respectively. This decreasing trend is consistent with the emission-reduction signal associated with anthropogenic pollution-control measures. Following the implementation of these policies, anthropogenic SO_2 emissions decreased by 63.14% per 20 years (Fig. 6(b),7(b)), leading to a parallel decrease in sulfate of 51.22% per 20 years (Fig. 6(e),7(b)). Aerosol liquid water, an important component of the reaction medium, also declines by 11.74% per 20 years (Fig. 6(f),7(b)) and further reinforces the downward trend in ISOA. Although biogenic isoprene emissions increase slightly by 4.54% per 20 years (Fig. 6(a),7(b)), this increase is insufficient to offset the overall weakening of the reaction medium and the associated formation environment. Consequently, surface ISOA shows a significant decline in SGN. Overall, the small change in the national-mean ISOA trend mainly results from pronounced regional heterogeneity and offsetting trends, and the dominant factors driving ISOA concentration changes differ substantially across regions.

To quantitatively diagnose the contributions of influential factors and better understand why ISOA trends differ between SWC and SGN, we constructed a multiple linear regression framework linking simulated monthly ISOA concentrations to key controlling factors. This regression framework was used in two complementary ways. Both analyses were based on regional monthly anomalies derived by first spatially averaging the original monthly gridded data over SWC and SGN to obtain regional-mean monthly time series and then removing the mean seasonal cycle. First, these monthly anomalies were standardized to zero mean and unit standard deviation to compare the relative statistical importance of different predictors on a common scale, as summarized in Text S1 and Table S1. This standardized analysis primarily diagnoses the leading predictors of month-to-month ISOA variability. Second, for the trend attribution diagnostic presented in Table 1, we used the same monthly anomalies without standardization, retaining the original physical units of each predictor. Multiple linear regression was subsequently applied to these unstandardized anomalies to obtain sensitivity coefficients in physical units. These sensitivity coefficients (α) describe how regional ISOA responds to changes in each predictor under the regression framework. For each predictor, its contribution to the simulated 20-year ISOA trend (C/20yr) was then estimated by multiplying its regression sensitivity by its own 20-year trend (dX/20yr). The relative contribution of each factor was further expressed as C/dY (%), where dY denotes the simulated 20-year ISOA trend in the corresponding region. The results show that the long-term increase in ISOA in SWC is most strongly associated with increasing biogenic isoprene emissions, resulting in an ISOA increase of 112.1 ng m^{-3} over 20 years, which corresponds to 58.29% of the total ISOA trend (Table 1). Sulfate has a positive sensitivity coefficient, but its concentration decreases over the study period, leading to a negative regression-based ISOA contribution of −74.18 ng m^{-3} over 20 years, which offsets the positive ISOA trend in SWC by 38.56%. In contrast, increasing anthropogenic NOx emissions are associated with a positive ISOA contribution of 32.86 ng m^{-3} over 20 years, although the corresponding regression coefficient is not statistically significant. Contributions from aerosol liquid water and $\log_{10}(H^+)$ are relatively small, with regression-based ISOA changes of −6.39 and 4.34 ng m^{-3} over

20 years, respectively (Table 1). In SGN, the long-term decrease in ISOA is mainly associated with declining sulfate, which contributes −84.38 ng m^{-3} over 20 years and accounts for 63.37% of the total ISOA decrease (Table 1). Despite increasing over the study period, anthropogenic NOx emissions are associated with an additional negative regression-based ISOA contribution of −45.25 ng m^{-3} over 20 years, corresponding to 33.98% of the total ISOA decrease, although this coefficient is not statistically significant and should therefore be interpreted cautiously. By comparison, increasing biogenic isoprene emissions partly offset the regional ISOA decline, resulting in a regression-based ISOA increase of 8.62 ng m^{-3} over 20 years, which offsets the total ISOA decrease by 6.48%. Aerosol liquid water also slightly offsets the ISOA decline, with a regression-based contribution of 5.66 ng m^{-3} over 20 years, corresponding to an offset of 4.25%, whereas $\log_{10}(H^+)$ contributes only weakly to the decrease, with a contribution of −0.72 ng m^{-3} over 20 years (Table 1). We further evaluated potential predictor correlations and collinearity by calculating pairwise Pearson correlation coefficients among the predictors used in the regression analysis (Fig. S9). The results indicate that some predictors are not fully independent. In both SWC and SGN, sulfate, aerosol liquid water, and $\log_{10}(H^+)$ show moderate to strong positive correlations, with correlation coefficients of 0.70–0.81 in SWC and 0.75–0.88 in SGN. These correlations are physically expected because aerosol liquid water is thermodynamically calculated in MOSAIC based on inorganic aerosol composition, including sulfate, as well as meteorological conditions. Sulfate also contributes to aerosol acidity and aerosol liquid water formation, while aerosol liquid water can further influence aqueous-phase uptake and processing. Therefore, sulfate, aerosol liquid water, and aerosol acidity are treated here as physically connected components of the aerosol chemical environment. Accordingly, the regression-based relative contributions associated with these covarying predictors should be interpreted as diagnostic indicators of statistical associations with ISOA variability, rather than as a strict decomposition of independent causal effects, because they may partly reflect coupled variations among sulfate, aerosol liquid water, and aerosol acidity. This caveat is less important for biogenic isoprene emissions and anthropogenic NOx emissions, as both predictors show weak correlations with the other predictors in both regions. Overall, these results suggest that the leading statistical predictors of long-term ISOA change differ between the two regions. The ISOA increase in SWC is primarily associated with enhanced biogenic isoprene emissions, while the ISOA decrease in SGN is most strongly associated with declining sulfate.~~To quantitatively diagnose the contributions from the influential factors and better understand why ISOA trends differ between SWC and SGN, we constructed a multiple linear regression framework linking simulated monthly ISOA concentrations to key controlling factors. Using this regression framework, we then quantified the contributions of individual drivers to the long-term ISOA trends in SWC and SGN by retaining the original physical units of all variables (Table 1). Specifically, we first spatially averaged the original monthly gridded data over SWC and SGN to obtain regional-mean monthly time series, and then removed the mean seasonal cycle to derive monthly anomalies. Multiple linear regression was subsequently applied to these unstandardized anomalies to obtain sensitivity coefficients in physical units. For each predictor, its long-term contribution to the ISOA trend was then estimated by combining its 20-year trend, dX/20 yr, with the corresponding regression sensitivity, yielding C/20 yr. The relative contribution of each factor was further expressed as C/dY (%), where dY/20 yr denotes the simulated 20-year trend in regional ISOA. The results show that the long-term increase in ISOA in SWC is primarily driven~~

~~by increasing biogenic isoprene emissions, resulting in an ISOA increase of 155.50 ng m^{-3} over 20 years, which accounts for 61.92% of the total ISOA trend (Table 1). Sulfate also led to an ISOA increase of 65.75–74.18 ng m^{-3} over 20 years, accounting for 26.17–38.56% of the total ISOA trend, whereas anthropogenic NOx emissions led to an ISOA change of −73.26–32.86 ng m^{-3} over 20 years. Contributions from aerosol liquid water and log10(H$^+$) are minor (Table 1). In contrast, the long-term decrease in ISOA in SGN is mainly associated with declining sulfate and increasing anthropogenic NOx emissions, which led to ISOA changes of −69.66 ng m^{-3} and −64.19 ng m^{-3} over 20 years, accounting for 48.96% and 45.11% of the total ISOA trend, respectively (Table 1). By comparison, increasing biogenic isoprene emissions partly offset the regional ISOA decline, resulting in an ISOA increase of 17.12 ng m^{-3} over 20 years, which accounts for 12.03% of the total ISOA trend. Aerosol liquid water and log10(H$^+$) play only minor roles, accounting for 2.70% and 2.47% of the total ISOA trend, respectively (Table 1). Overall, these results further demonstrate that the dominant drivers of long-term ISOA change differ fundamentally between the two regions, with enhanced biogenic isoprene emissions dominating the increase in SWC and anthropogenic NOx emissions together with sulfate changes driving the decrease in SGN.~~

Driver	Southwest China (SWC)					Shaanxi–Gansu–Ningxia region (SGN)				
	dX/20yr	α	p_α	C/20yr	C/dY (%)	dX/20yr	α	p_α	C/20yr	C/dY (%)
ISOP emis (g/m^2/mon)	0.028	4074	0.001	112.1	**58.29**	0.005	1618	0.043	8.622	-6.480
SO_4^{2-} (μg/m^3)	-1.529	48.53	0.126	-74.18	-38.56	-3.525	23.94	0.049	-84.38	**63.37**
Anthro NOx emis (g/m^2/mon)	0.033	1006	0.632	32.86	17.08	0.081	-553.0	0.271	-45.25	33.98
AeroWater (μg/m^3)	-2.004	3.188	0.622	-6.387	-3.320	-2.834	-1.997	0.554	5.658	-4.250
$log_{10}(H^+)$	-0.109	-39.70	0.901	4.336	2.250	-0.015	46.48	0.618	-0.715	0.540

Table 1: Regression-based attribution of long-term ISOA trends in Southwest China (SWC) and the Shaanxi–Gansu–Ningxia region (SGN). The regression is based on deseasonalized monthly anomalies from the simulation years, and the resulting sensitivity coefficients are combined with the changes in individual drivers over 2000–2019 to estimate their contributions to the long-term ISOA trend. For each driver, the table lists its 20-year change (dX/20 yr), regression sensitivity coefficient (α), significance level (p_α), attributed contribution to the ISOA trend (C/20 yr), and relative contribution (C/dY; %). Bold values indicate the largest relative contributions in each region.

We also examined the interannual evolution of the four major ISOA subspecies in SWC and SGN over 2000–2019, and the detailed results are presented in Fig. 8. The two regions show clearly different interannual changes in ISOA subspecies, consistent with the contrasting regional ISOA trends discussed above. In SWC, all four ISOA subspecies increase from 2000 to 2006 (Fig. 8(a)). This increase is consistent with the simultaneous increases in biogenic isoprene emissions (Fig. 8(b)), epoxide precursor concentrations (Fig. 8(c)), and particle-phase reaction conditions, including sulfate and aerosol liquid

water (Fig. 8(d)), during the same period. After 2006, most ISOA subspecies generally decrease toward 2016, whereas AHMGA shows a delayed maximum in 2012, mainly reflecting the combined effects of elevated anthropogenic NOx emissions, enhanced HMML + MAE precursor concentrations, and the peak in aerosol liquid water that favors H_2O-mediated heterogeneous uptake. This is followed by a rebound in the normalized values of all four ISOA subspecies from 2016 to 2019. Notably, this rebound occurs despite the continued decreases in anthropogenic SO_2 emissions, sulfate, and aerosol liquid water after 2012, suggesting that precursor supply and epoxide precursor concentrations play a stronger role in driving the later-stage ISOA recovery in SWC. This feature is also consistent with the multiple linear regression results discussed above, which identify biogenic isoprene emissions as the leading statistical indicator of ISOA variability and long-term changes in SWC. In contrast, ISOA subspecies in SGN generally peak in 2006 and decline thereafter, showing a more synchronous temporal evolution across different product classes. This decline in ISOA subspecies after 2006 occurs even though biogenic isoprene emissions and gas-phase epoxide precursor concentrations increase over the same period, suggesting that declining sulfate and aerosol liquid water can constrain heterogeneous uptake and particle-phase product formation in SGN. These patterns suggest that the temporal evolution in SGN is more strongly linked to changes in the aerosol reaction medium. This interpretation is also consistent with the multiple linear regression results discussed above, which identify sulfate as the leading statistical indicator and the dominant regression-based contributor to the long-term ISOA decrease in SGN. These regional differences indicate that the mechanisms governing ISOA changes are not spatially uniform and provide additional process-based support for the contrasting ISOA trends identified in SWC and SGN.~~We also examined the interannual evolution of the four major ISOA subspecies in SWC and SGN over 2000–2019, and the detailed results are presented in the Supplement and Fig. 8. The temporal behavior of pathway-specific products differs clearly between the two regions, further supporting the distinct controls inferred from the trend attribution analysis. In SWC, low-NOx products peak in 2006, whereas high-NOx products reach their maxima later, in 2012, indicating a clear separation in the temporal responses of the two formation pathways. This pattern suggests that precursor supply plays a stronger role in shaping the peak timing and concentration evolution in SWC. In contrast, in SGN, products from both pathways generally peak in 2006 and decline thereafter, showing a more synchronous temporal evolution, which indicates that sulfate-related heterogeneous reaction conditions exert stronger control on their peak timing and subsequent changes. These differences suggest that the mechanisms governing ISOA changes are not spatially uniform and provide additional process-based support for the contrasting regional trends identified in SWC and SGN.~~

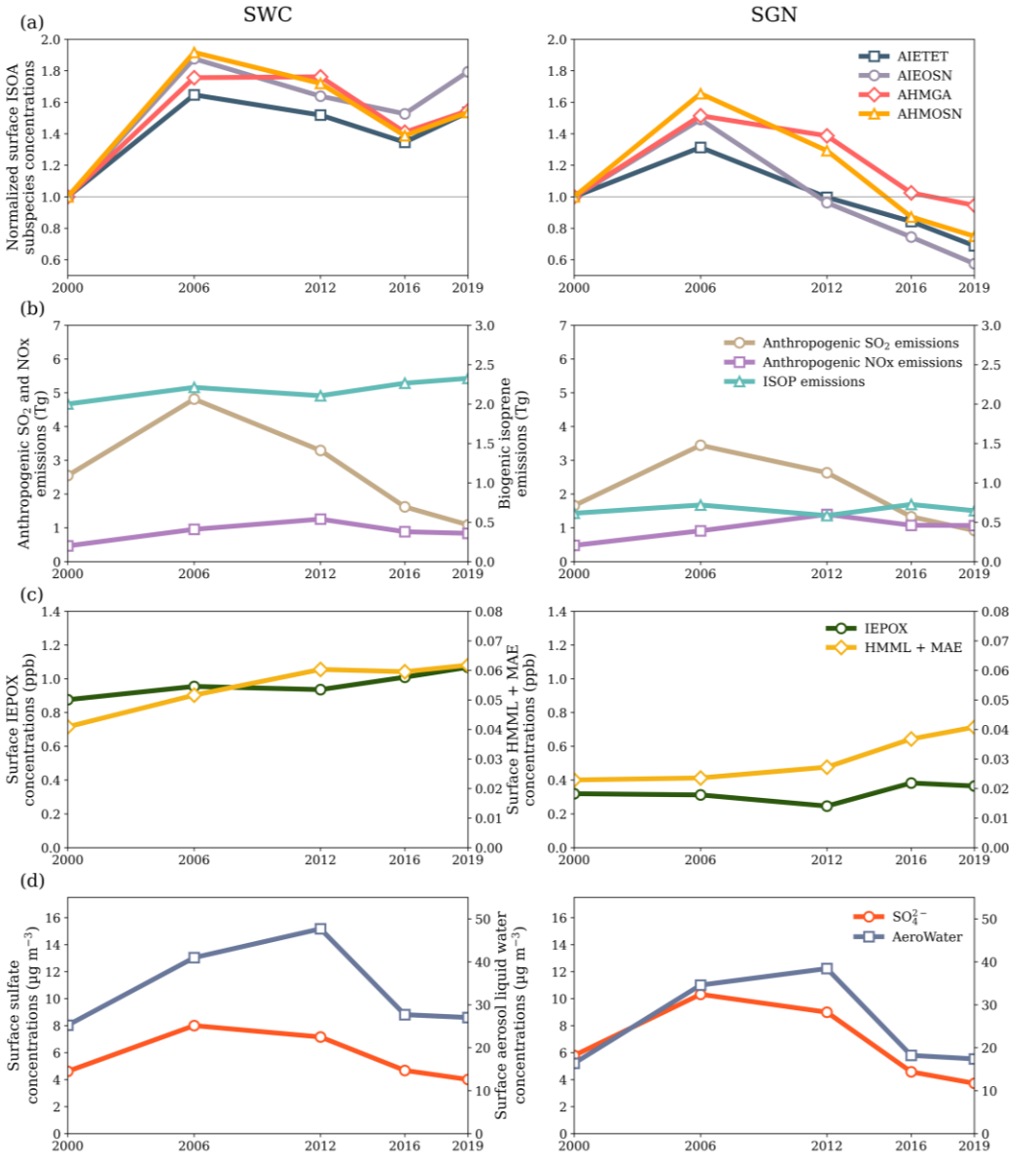

Figure 8: Time series for Southwest China (SWC; left column) and the Shaanxi–Gansu–Ningxia region (SGN; right column), showing (a) normalized surface isoprene-derived secondary organic aerosol (ISOA) subspecies concentrations, including AIETET (dark blue), AIEOSN (gray-purple), AHMGA (rose red), and AHMOSN (earthy yellow). The normalized values are calculated as the ratio of the value in each year to that in 2000; (b) anthropogenic sulfur dioxide (SO_2) emissions (tan; left y axis; unit: Tg) and anthropogenic nitrogen oxides (NOx) emissions (purple; left y axis; unit: Tg), and biogenic isoprene emissions (blue; right y axis; unit: Tg); (c) surface isoprene epoxydiols (IEPOX) concentrations (dark green; left y axis; unit: ppb) and surface hydroxymethyl-methyl-α-lactone plus methacrylic acid epoxide (HMML + MAE) concentrations (yellow; right y axis; unit: ppb); and (d) surface sulfate (SO_4^{2-}) concentrations (red-orange; left y axis; unit: μg m^{-3}) and surface aerosol liquid water (AeroWater) concentrations (blue-gray; right y axis; unit: μg m^{-3}).

Taken together, the contrasting ISOA trends in SWC and SGN highlight the need for a coupled precursor–multiphase reaction framework. The SWC case represents a more precursor-driven regime, in which enhanced biogenic isoprene emissions and NOx-dependent oxidation promote epoxide precursor formation and enhance ISOA production despite less favorable aerosol multiphase reaction conditions. In contrast, the SGN case represents a more reaction-medium-limited regime, in which declining sulfate and aerosol liquid water suppress heterogeneous uptake and particle-phase product formation, even when precursor supply or NOx levels remain relatively high. This regime-based interpretation emphasizes the balance between precursor supply, NOx-dependent oxidation chemistry, and aerosol multiphase reaction conditions, as summarized schematically in Fig. 9.

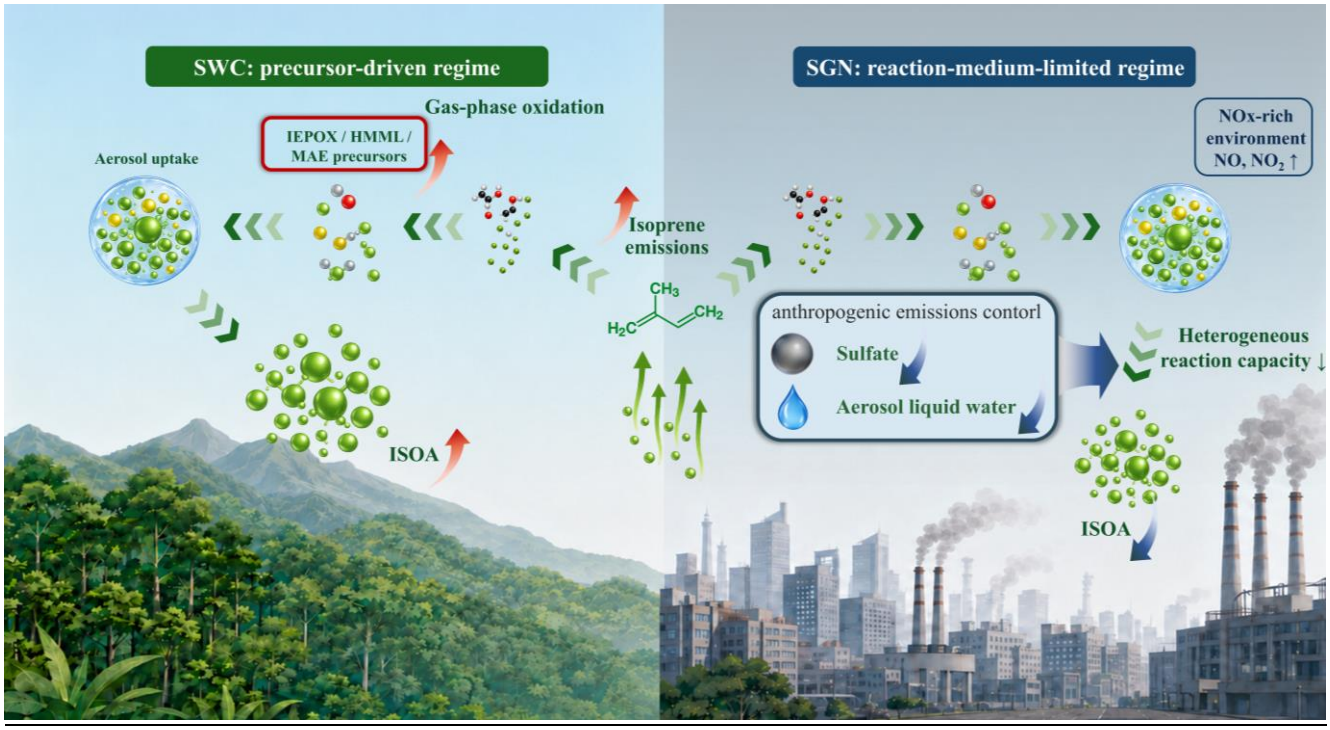

Figure 9. Schematic illustration of contrasting regional controls on surface isoprene-derived secondary organic aerosol (ISOA) formation in Southwest China (SWC; left) and the Shaanxi–Gansu–Ningxia region (SGN; right). The background scenes and selected graphical elements were created with the assistance of OpenAI's image-generation tools in ChatGPT (OpenAI, 2026).

4. Conclusions and Discussions

This study implements an explicit ISOA formation mechanism in CAM6-Chem that introduces representations of high-NOx epoxide precursors and their heterogeneous uptake, while resolving reactive-uptake-derived ISOA into H_2O-mediated nucleophilic addition and inorganic-nucleophile-addition product classes. Evaluation against ground-based observations

shows that the explicit ISOA mechanism better reproduces the concentrations and compositional structure of major ISOA subspecies, although positive biases remain for AIETET and AHMGA. At the bulk aerosol level, this mechanism substantially alleviates the underestimation of SOA and OA over China, with the NMB improving from −76.7% to −51.6% for SOA and from −47.0% to −25.7% for OA. In addition, the explicit simulation better captures the observed multi-component nature of ambient ISOA and better reproduces the relative contributions of subspecies associated with the newly introduced pathways. These results demonstrate that the explicit ISOA mechanism is chemically meaningful and improves the model's ability to represent both the magnitude and composition of ambient ISOA.~~This study updates the explicit isoprene oxidation scheme in CAM6-Chem by introducing a more complete representation of both low-NOx and high-NOx ISOA formation pathways. Specifically, the updated mechanism adds IEPOX reactive uptake to aerosol liquid water under low-NOx conditions and incorporates the key gas-phase precursors and subsequent heterogeneous processes under high-NOx conditions. Evaluation against ground-based observations shows that the updated model better reproduces the concentrations and compositional structure of major ISOA subspecies, although positive biases remain for AIETET and AHMGA. At the bulk aerosol level, the mechanism update substantially alleviates the underestimation of SOA and OA over China, with the NMB improving from −76.7% to −50.0% for SOA and from −47.0% to −24.5% for OA. In addition, the updated simulation more successfully captures the observed multi-component nature of ambient ISOA and better reproduces the relative contributions of subspecies associated with the newly introduced pathways. These results demonstrate that the mechanism update is chemically meaningful and improves the model's ability to represent both the magnitude and composition of ambient ISOA.~~

Using this explicit ISOA framework~~Using this updated framework~~, we find that ISOA formation in China reflects competition between the IEPOX pathway and the MAE/HMML pathway under different NOx backgrounds. On the national average, the IEPOX pathway remains the dominant source of ISOA, with an annual mean $ISOA_{HMML+MAE}/ISOA_{IEPOX}$ ratio of only about 0.07. The relative importance of the MAE/HMML pathway increases in NOx-rich regions and during late summer to early autumn, reaching a seasonal maximum in September, but it remains secondary to IEPOX even under these conditions. Overall, these results indicate that NOx enhances the contribution of the MAE/HMML pathway regionally and seasonally, while the IEPOX pathway continues to dominate ISOA formation at the national scale.

Against this national-scale background, spatial analysis showed that the long-term national-mean change in surface ISOA over China during 2000–2019 was weak, largely because strong regional trends with opposite signs offset each other. The most pronounced increase occurred in SWC, whereas the strongest decrease occurred in SGN. Regression-based attribution further showed that the ISOA increase in SWC was most strongly associated with enhanced biogenic isoprene emissions, while the ISOA decrease in SGN was mainly associated with declining sulfate. These contrasts were also reflected in the normalized interannual evolution of major ISOA subspecies. In SWC, the normalized values of all four ISOA subspecies rebounded from 2016 to 2019 despite the post-2012 decreases in sulfate and aerosol liquid water, suggesting an important

role of precursor supply. In SGN, by contrast, ISOA subspecies generally peaked in 2006 and declined thereafter, even though biogenic isoprene emissions and gas-phase epoxide precursor concentrations increased after 2006, highlighting the stronger constraint from weakened aerosol multiphase reaction conditions. Together, these results demonstrate that long-term ISOA changes in China are governed by different regional balances between precursor availability and aerosol multiphase reaction conditions.~~Against this national-scale background, spatial analysis showed that the long-term national-mean change in surface ISOA over China during 2000–2019 was weak, largely because strong regional trends with opposite signs offset each other. The most pronounced increase occurred in SWC, whereas the strongest decrease occurred in SGN. Regression-based attribution further revealed clear regional contrasts in the dominant drivers of ISOA change. In SWC, the ISOA increase was most strongly associated with enhanced biogenic isoprene emissions, whereas in SGN, the decrease was mainly associated with declining sulfate. These regional differences were also reflected in the temporal evolution of major ISOA subspecies. In SWC, the four ISOA subspecies increased from 2000 to 2006 and rebounded by 2019 despite the post-2012 decreases in sulfate and aerosol liquid water, suggesting an important role of precursor supply. In SGN, by contrast, ISOA subspecies generally peaked in 2006 and declined thereafter, even though biogenic isoprene emissions and gas-phase epoxide precursor concentrations increased after 2006, highlighting the stronger constraint from the weakening aerosol reaction medium. Together, these results demonstrate that long-term ISOA changes in China are governed by strong regional heterogeneity and by differing interactions between precursor availability and reaction-medium conditions.~~

Future model development should further address several simplifying assumptions in the current epoxide reactive uptake parameterization. As described in Sect. 2.1.2, the model follows a core-shell treatment in which the organic shell and aqueous core are assumed to have the same reaction rate coefficient. Because phase separation and increased organic-shell viscosity can limit epoxide diffusion and reactive uptake, this assumption may overestimate epoxide-derived ISOA under strongly phase-separated or highly viscous conditions (Zhang et al., 2019; Schmedding et al., 2020; Chen et al., 2024; Farrell et al., 2025). HMML and MAE are also represented using the same solubility, diffusivity, and condensed-phase reaction parameters as IEPOX because compound-specific laboratory constraints remain limited. This IEPOX-like treatment introduces uncertainty in the absolute uptake rates of high-NOx epoxides and in the quantitative $ISOA_{HMML+MAE}/ISOA_{IEPOX}$ ratio. The assumptions of 100 % SOA yield from epoxide reactive uptake and non-volatile epoxide-derived SOA introduce additional uncertainty. Although these assumptions are consistent with previous global ISOA modeling studies (Marais et al., 2016; Jo et al., 2019, 2021), lower effective yields or partial volatility, especially for products such as 2-MT and 2-MGA, could reduce simulated ISOA concentrations and their sensitivity to sulfate, aerosol liquid water, and acidity. Finally, the removal of ISOA formation from the VBS scheme may also remove important non-epoxide contributions to ISOA that were previously represented implicitly, such as multifunctional organic peroxides under low-NOx conditions and organic nitrates under high-NOx conditions. Taken together, these assumptions mean that the long-term trends and regression-based attributions diagnosed here should be interpreted within the adopted epoxide-focused chemical framework, rather than as exact causal contributions independent of model structure and parameterization.

Beyond the uncertainties associated with parameterizations already included in the current framework, some potentially important ISOA processes remain absent from the model. These include isoprene cloud-water chemistry, which may provide an additional ISOA source and influence simulated aerosol composition, and photolytic loss, since ISOA may photolyze faster than monoterpene-derived SOA (Zawadowicz et al., 2020), thereby affecting its simulated lifetime and burden. Incorporating these missing formation and loss processes, together with more composition-resolved observations to constrain pathway-specific chemistry, will be important for future model refinement. Future global-scale simulations and attribution analyses would also be useful for evaluating whether the updated ISOA mechanism has broader implications for other high-isoprene regions, where climate change and human activities may shift the relative roles of biogenic precursor supply, anthropogenic emissions, and the heterogeneous aerosol reaction environment in shaping future ISOA responses. ~~Despite these advances, the current model may still have limitations in both the emissions inventories and the chemical mechanism used to simulate SOA. In particular, CAM6-Chem does not explicitly include isoprene cloud-water chemistry, which may provide an additional source of ISOA and could influence both the magnitude and composition of simulated aerosols. Further refinement of the chemical mechanism is therefore needed to improve model performance and reduce the remaining biases in key ISOA subspecies. At the same time, more composition-resolved observations are needed to better constrain pathway-specific formation processes and to further clarify the coupled influences of biogenic and anthropogenic factors on ISOA.~~

Code and data availability

The Community Earth System Model (CESM) is an open-source framework available at https://www.cesm.ucar.edu/models/cesm2/download. The modified code for the explicit isoprene chemistry scheme implemented in this study is available upon reasonable request. Ground-based measurements for OA and SOA were obtained from the supplementary materials of published articles by Miao et al. (2021) and Chen et al. (2024a). Ground-based measurements of AIETET and AHMGA were obtained from Ding et al. (2016). Ground-based measurements of ISOA products used to evaluate ISOA composition and pathway partitioning were obtained from Zhang et al. (2022).

Author contributions

XD, MW, and WZ designed the study. WZ developed the model code, performed the simulations, produced the figures, and wrote the manuscript draft. MY and XS contributed to the model simulations. All the authors contributed to the discussion and editing of the manuscript.

Competing interests

At least one of the (co-)authors is a member of the editorial board of Atmospheric Chemistry and Physics.

Acknowledgements

We appreciate the High Performance Computing Center of Nanjing University for providing the computational resources essential for this research. We are also grateful to the anonymous reviewers for their valuable comments and constructive suggestions, which helped improve the quality of the paper. The background scenes and selected graphical elements in Fig. 9 were created with the assistance of OpenAI's image-generation tools in ChatGPT (OpenAI, 2026).~~We appreciate the High Performance Computing Center of Nanjing University for providing the computational resources essential for this research. Additionally, we are grateful to the anonymous reviewers for their valuable feedback and suggestions aimed at enhancing the quality of the paper.~~

Financial support

This work acknowledges financial support from the National Natural Science Foundation of China (grant nos. 42575126 and 42505184~~grant no. 42575126~~) and the Collaborative Innovation Center of Climate Change, Jiangsu Province.

References

Bardakov, R., Thornton, J. A., Riipinen, I., Krejci, R., and Ekman, A. M. L.: Transport and chemistry of isoprene and its oxidation products in deep convective clouds, Tellus B: Chemical and Physical Meteorology, 73, 1979856, https://doi.org/10.1080/16000889.2021.1979856, 2021.

Birdsall, A. W., Miner, C. R., Mael, L. E., and Elrod, M. J.: Mechanistic study of secondary organic aerosol components formed from nucleophilic addition reactions of methacrylic acid epoxide, Atmos. Chem. Phys., 14, 12951–12964, https://doi.org/10.5194/acp-14-12951-2014, 2014.

Budisulistiorini, S. H., Li, X., Bairai, S. T., Renfro, J., Liu, Y., Liu, Y. J., McKinney, K. A., Martin, S. T., McNeill, V. F., Pye, H. O. T., Nenes, A., Neff, M. E., Stone, E. A., Mueller, S., Knote, C., Shaw, S. L., Zhang, Z., Gold, A., and Surratt, J. D.: Examining the effects of anthropogenic emissions on isoprene-derived secondary organic aerosol formation during the 2013 Southern Oxidant and Aerosol Study (SOAS) at the Look Rock, Tennessee ground site, Atmos. Chem. Phys., 15, 8871–8888, https://doi.org/10.5194/acp-15-8871-2015, 2015.

Budisulistiorini, S. H., Nenes, A., Carlton, A. G., Surratt, J. D., McNeill, V. F., and Pye, H. O. T.: Simulating aqueous-phase isoprene-epoxydiol (IEPOX) secondary organic aerosol production during the 2013 Southern Oxidant and Aerosol Study (SOAS), Environ. Sci. Technol., 51, 5026–5034, https://doi.org/10.1021/acs.est.6b05750, 2017.

Carlton, A. G., Bhave, P. V., Napelenok, S. L., Edney, E. O., Sarwar, G., Pinder, R. W., Pouliot, G. A., and Houyoux, M.: Model representation of secondary organic aerosol in CMAQv4.7, Environ. Sci. Technol., 44, 8553–8560, https://doi.org/10.1021/es100636q, 2010.

Carlton, A. G., Wiedinmyer, C., and Kroll, J. H.: A review of Secondary Organic Aerosol (SOA) formation from isoprene, Atmos. Chem. Phys., 9, 4987–5005, https://doi.org/10.5194/acp-9-4987-2009, 2009.

Chang, X., Zhao, B., Zheng, H., Wang, S., Cai, S., Guo, F., Gui, P., Huang, G., Wu, D., Han, L., Xing, J., Man, H., Hu, R., Liang, C., Xu, Q., Qiu, X., Ding, D., Liu, K., Han, R., Robinson, A. L., and Donahue, N. M.: Full-volatility emission framework corrects missing and underestimated secondary organic aerosol sources, One Earth, 5, 403–412, https://doi.org/10.1016/j.oneear.2022.03.015, 2022.

Chen, Q., Miao, R., Geng, G., Shrivastava, M., Dao, X., Xu, B., Sun, J., Zhang, X., Liu, M., Tang, G., Tang, Q., Hu, H., Huang, R.-J., Wang, H., Zheng, Y., Qin, Y., Guo, S., Hu, M., and Zhu, T.: Widespread 2013–2020 decreases and reduction challenges of organic aerosol in China, Nat. Commun., 15, 4465, https://doi.org/10.1038/s41467-024-48902-0, 2024a.

Chen, Y., Ng, A. E., Green, J., Zhang, Y., Riva, M., Riedel, T. P., Pye, H. O. T., Lei, Z., Olson, N. E., Cooke, M. E., Zhang, Z., Vizuete, W., Gold, A., Turpin, B. J., Ault, A. P., and Surratt, J. D.: Applying a Phase-Separation Parameterization in Modeling Secondary Organic Aerosol Formation from Acid-Driven Reactive Uptake of Isoprene Epoxydiols under Humid Conditions, ACS ES&T Air, 1, 511–524, https://doi.org/10.1021/acsestair.4c00002, 2024b.

Chin, M., Ginoux, P., Kinne, S., Torres, O., Holben, B. N., Duncan, B. N., Martin, R. V., Logan, J. A., Higurashi, A., and Nakajima, T.: Tropospheric aerosol optical thickness from the GOCART model and comparisons with satellite and sun photometer measurements, J. Atmos. Sci., 59, 461–483, https://doi.org/10.1175/1520-0469(2002)059<0461:TAOTFT>2.0.CO;2, 2002.

Chung, S. H. and Seinfeld, J. H.: Global distribution and climate forcing of carbonaceous aerosols, J. Geophys. Res.-Atmos., 107, 4407, https://doi.org/10.1029/2001JD001397, 2002.

Ding, X., He, Q.-F., Shen, R.-Q., Yu, Q.-Q., and Wang, X.-M.: Spatial distributions of secondary organic aerosols from isoprene, monoterpenes, β-caryophyllene, and aromatics over China during summer: secondary organic aerosols over China, J. Geophys. Res.-Atmos., 119, 11877–11891, https://doi.org/10.1002/2014JD021748, 2014.

Ding, X., He, Q.-F., Shen, R.-Q., Yu, Q.-Q., Zhang, Y.-Q., Xin, J.-Y., Wen, T.-X., and Wang, X.-M.: Spatial and seasonal variations of isoprene secondary organic aerosol in China: Significant impact of biomass burning during winter, Sci. Rep., 6, 20411, https://doi.org/10.1038/srep20411, 2016.

Donahue, N. M., Robinson, A. L., Stanier, C. O., and Pandis, S. N.: Coupled partitioning, dilution, and chemical aging of semivolatile organics, Environ. Sci. Technol., 40, 2635–2643, https://doi.org/10.1021/es052297c, 2006.

Dong, X., Liu, Y., Li, X., Yue, M., Liu, Y., Ma, Z., Zheng, H., Huang, R., and Wang, M.: Modeling Analysis of Biogenic Secondary Organic Aerosol Dependence on Anthropogenic Emissions in China, Environ. Sci. Technol. Lett., 9, 286–292, https://doi.org/10.1021/acs.estlett.2c00104, 2022.

Eddingsaas, N. C., VanderVelde, D. G., and Wennberg, P. O.: Kinetics and Products of the Acid-Catalyzed Ring-Opening of Atmospherically Relevant Butyl Epoxy Alcohols, J. Phys. Chem. A, 114, 8106–8113, https://doi.org/10.1021/jp103907c, 2010.

Emmons, L. K., Schwantes, R. H., Orlando, J. J., Tyndall, G., Kinnison, D., Lamarque, J., Marsh, D., Mills, M. J., Tilmes, S., Bardeen, C., Buchholz, R. R., Conley, A., Gettelman, A., Garcia, R., Simpson, I., Blake, D. R., Meinardi, S., and Pétron, G.: The Chemistry Mechanism in the Community Earth System Model Version 2 (CESM2), J. Adv. Model. Earth Syst., 12, e2019MS001882, https://doi.org/10.1029/2019MS001882, 2020.

Fahey, K. M., Carlton, A. G., Pye, H. O. T., Baek, J., Hutzell, W. T., Stanier, C. O., Baker, K. R., Appel, K. W., Jaoui, M., and Offenberg, J. H.: A framework for expanding aqueous chemistry in the Community Multiscale Air Quality (CMAQ) model version 5.1, Geosci. Model Dev., 10, 1587–1605, https://doi.org/10.5194/gmd-10-1587-2017, 2017.

Farrell, S. L., Rasool, Q. Z., Pye, H. O. T., Zhang, Y., Li, Y., Chen, Y., Wang, C. T., Zhang, H., Schmedding, R., Shiraiwa, M., Greene, J., Budisulistiorini, S. H., Jimenez, J. L., Hu, W., Surratt, J. D., and Vizuete, W. C.: Simulated reductions in heterogeneous isoprene epoxydiol reactive uptake from aerosol morphology in the contiguous United States using the Community Multiscale Air Quality Model (CMAQ v5.3.2), EGUsphere [preprint], https://doi.org/10.5194/egusphere-2025-2253, 2025.

Gaston, C. J., Thornton, J. A., and Ng, N. L.: Reactive uptake of N_2O_5 to internally mixed inorganic and organic particles: the role of organic carbon oxidation state and inferred organic phase separations, Atmos. Chem. Phys., 14, 5693–5707, https://doi.org/10.5194/acp-14-5693-2014, 2014.

Gelaro, R., McCarty, W., Suárez, M. J., Todling, R., Molod, A., Takacs, L., Randles, C. A., Darmenov, A., Bosilovich, M. G., Reichle, R., Wargan, K., Coy, L., Cullather, R., Draper, C., Akella, S., Buchard, V., Conaty, A., Da Silva, A. M., Gu, W., Kim, G.-K., Koster, R., Lucchesi, R., Merkova, D., Nielsen, J. E., Partyka, G., Pawson, S., Putman, W., Rienecker, M., Schubert, S. D., Sienkiewicz, M., and Zhao, B.: The Modern-Era Retrospective Analysis for Research and Applications, Version 2 (MERRA-2), J. Climate, 30, 5419–5454, https://doi.org/10.1175/JCLI-D-16-0758.1, 2017.

Gettelman, A. and Morrison, H.: Advanced Two-Moment Bulk Microphysics for Global Models. Part I: Off-Line Tests and Comparison with Other Schemes, J. Climate, 28, 1268–1287, https://doi.org/10.1175/JCLI-D-14-00102.1, 2015.

Griffin, R. J., Cocker, D. R., III, Flagan, R. C., and Seinfeld, J. H.: Organic aerosol formation from the oxidation of biogenic hydrocarbons, J. Geophys. Res.-Atmos., 104, 3555–3567, https://doi.org/10.1029/1998JD100049, 1999.

Guenther, A. B., Jiang, X., Heald, C. L., Sakulyanontvittaya, T., Duhl, T., Emmons, L. K., and Wang, X.: The Model of Emissions of Gases and Aerosols from Nature version 2.1 (MEGAN2.1): an extended and updated framework for modeling biogenic emissions, Geosci. Model Dev., 5, 1471–1492, https://doi.org/10.5194/gmd-5-1471-2012, 2012.

He, Q.-F., Ding, X., Fu, X.-X., Zhang, Y.-Q., Wang, J.-Q., Liu, Y.-X., Tang, M.-J., Wang, X.-M., and Rudich, Y.: Secondary organic aerosol formation from isoprene epoxides in the Pearl River Delta, South China: IEPOX- and HMML-derived tracers, J. Geophys. Res.-Atmos., 123, 6999–7012, https://doi.org/10.1029/2017JD028242, 2018.

Hodzic, A., Kasibhatla, P. S., Jo, D. S., Cappa, C. D., Jimenez, J. L., Madronich, S., and Park, R. J.: Rethinking the global secondary organic aerosol (SOA) budget: stronger production, faster removal, shorter lifetime, Atmos. Chem. Phys., 16, 7917–7941, https://doi.org/10.5194/acp-16-7917-2016, 2016.

Hu, H., Liang, Y., Li, T., She, Y., Wang, Y., Yang, T., Zhou, M., Li, Z., Li, C., Xiao, H., Hu, J., Li, J., and Zhao, Y.: Pathway-specific responses of isoprene-derived secondary organic aerosol formation to anthropogenic emission reductions in a megacity in eastern China, Atmos. Chem. Phys., 25, 17889–17906, https://doi.org/10.5194/acp-25-17889-2025, 2025.

Hu, W. W., Campuzano-Jost, P., Palm, B. B., Day, D. A., Ortega, A. M., Hayes, P. L., Krechmer, J. E., Chen, Q., Kuwata, M., Liu, Y. J., De Sá, S. S., McKinney, K., Martin, S. T., Hu, M., Budisulistiorini, S. H., Riva, M., Surratt, J. D., St. Clair, J. M., Isaacman-Van Wertz, G., Yee, L. D., Goldstein, A. H., Carbone, S., Brito, J., Artaxo, P., De Gouw, J. A., Koss, A., Wisthaler, A., Mikoviny, T., Karl, T., Kaser, L., Jud, W., Hansel, A., Docherty, K. S., Alexander, M. L., Robinson, N. H., Coe, H., Allan, J. D., Canagaratna, M. R., Paulot, F., and Jimenez, J. L.: Characterization of a real-time tracer for isoprene epoxydiols-derived secondary organic aerosol (IEPOX-SOA) from aerosol mass spectrometer measurements, Atmos. Chem. Phys., 15, 11807–11833, https://doi.org/10.5194/acp-15-11807-2015, 2015.

Hu, W., Palm, B. B., Day, D. A., Campuzano-Jost, P., Krechmer, J. E., Peng, Z., De Sá, S. S., Martin, S. T., Alexander, M. L., Baumann, K., Hacker, L., Kiendler-Scharr, A., Koss, A. R., De Gouw, J. A., Goldstein, A. H., Seco, R., Sjostedt, S. J., Park, J.-H., Guenther, A. B., Kim, S., Canonaco, F., Prévôt, A. S. H., Brune, W. H., and Jimenez, J. L.: Volatility and lifetime against OH heterogeneous reaction of ambientisoprene-epoxydiols-derived secondary organic aerosol (IEPOX-SOA), Atmos. Chem. Phys., 16, 11563–11580, https://doi.org/10.5194/acp-16-11563-2016, 2016.

Jo, D. S., Hodzic, A., Emmons, L. K., Marais, E. A., Peng, Z., Nault, B. A., Hu, W., Campuzano-Jost, P., and Jimenez, J. L.: A simplified parameterization of isoprene-epoxydiol-derived secondary organic aerosol (IEPOX-SOA) for global chemistry and climate models: a case study with GEOS-Chem v11-02-rc, Geosci. Model Dev., 12, 2983–3000, https://doi.org/10.5194/gmd-12-2983-2019, 2019.

Jo, D. S., Hodzic, A., Emmons, L. K., Tilmes, S., Schwantes, R. H., Mills, M. J., Campuzano-Jost, P., Hu, W., Zaveri, R. A., Easter, R. C., Singh, B., Lu, Z., Schulz, C., Schneider, J., Shilling, J. E., Wisthaler, A., and Jimenez, J. L.: Future changes in isoprene-epoxydiol-derived secondary organic aerosol (IEPOX SOA) under the Shared Socioeconomic Pathways: the importance of physicochemical dependency, Atmos. Chem. Phys., 21, 3395–3425, https://doi.org/10.5194/acp-21-3395-2021, 2021.

Kim, P. S., Jacob, D. J., Fisher, J. A., Travis, K., Yu, K., Zhu, L., Yantosca, R. M., Sulprizio, M. P., Jimenez, J. L., Campuzano-Jost, P., Froyd, K. D., Liao, J., Hair, J. W., Fenn, M. A., Butler, C. F., Wagner, N. L., Gordon, T. D., Welti, A., Wennberg, P. O., Crounse, J. D., St. Clair, J. M., Teng, A. P., Millet, D. B., Schwarz, J. P., Markovic, M. Z., and Perring, A. E.: Sources, seasonality, and trends of southeast US aerosol: an integrated analysis of surface, aircraft, and satellite observations with the GEOS-Chem chemical transport model, Atmos. Chem. Phys., 15, 10411–10433, https://doi.org/10.5194/acp-15-10411-2015, 2015.

Li, J., Wang, G., Wu, C., Cao, C., Ren, Y., Wang, J., Li, J., Cao, J., Zeng, L., and Zhu, T.: Characterization of isoprene-derived secondary organic aerosols at a rural site in North China Plain with implications for anthropogenic pollution effects, Sci. Rep., 8, 535, https://doi.org/10.1038/s41598-017-18983-7, 2018.

Li, M., Liu, H., Geng, G., Hong, C., Liu, F., Song, Y., Tong, D., Zheng, B., Cui, H., Man, H., Zhang, Q., and He, K.: Anthropogenic emission inventories in China: a review, Natl. Sci. Rev., 4, 834–866, https://doi.org/10.1093/nsr/nwx150, 2017.

Lin, Y.-H., Zhang, H., Pye, H. O. T., Zhang, Z., Marth, W. J., Park, S., Arashiro, M., Cui, T., Budisulistiorini, S. H., Sexton, K. G., Vizuete, W., Xie, Y., Luecken, D. J., Piletic, I. R., Edney, E. O., Bartolotti, L. J., Gold, A., and Surratt, J. D.: Epoxide as a precursor to secondary organic aerosol formation from isoprene photooxidation in the presence of nitrogen oxides, Proc. Natl. Acad. Sci. USA, 110, 6718–6723, https://doi.org/10.1073/pnas.1221150110, 2013.

Lin, Y.-H., Zhang, Z., Docherty, K. S., Zhang, H., Budisulistiorini, S. H., Rubitschun, C. L., Shaw, S. L., Knipping, E. M., Edgerton, E. S., Kleindienst, T. E., Gold, A., and Surratt, J. D.: Isoprene Epoxydiols as Precursors to Secondary Organic Aerosol Formation: Acid-Catalyzed Reactive Uptake Studies with Authentic Compounds, Environ. Sci. Technol., 46, 250–258, https://doi.org/10.1021/es202554c, 2012.

Liu, X., Ma, P.-L., Wang, H., Tilmes, S., Singh, B., Easter, R. C., Ghan, S. J., and Rasch, P. J.: Description and evaluation of a new four-mode version of the Modal Aerosol Module (MAM4) within version 5.3 of the Community Atmosphere Model, Geosci. Model Dev., 9, 505–522, https://doi.org/10.5194/gmd-9-505-2016, 2016.

Liu, Y., Dong, X., Emmons, L. K., Jo, D. S., Liu, Y., Shrivastava, M., Yue, M., Liang, Y., Song, Z., He, X., and Wang, M.: Exploring the Factors Controlling the Long-Term Trend (1988–2019) of Surface Organic Aerosols in the Continental United States by Simulations, J. Geophys. Res.-Atmos., 128, e2022JD037935, https://doi.org/10.1029/2022JD037935, 2023.

Lu, Z., Liu, X., Zaveri, R. A., Easter, R. C., Tilmes, S., Emmons, L. K., Vitt, F., Singh, B., Wang, H., Zhang, R., and Rasch, P. J.: Radiative Forcing of Nitrate Aerosols From 1975 to 2010 as Simulated by MOSAIC Module in CESM2-MAM4, J. Geophys. Res.-Atmos., 126, e2021JD034809, https://doi.org/10.1029/2021JD034809, 2021.

Marais, E. A., Jacob, D. J., Jimenez, J. L., Campuzano-Jost, P., Day, D. A., Hu, W., Krechmer, J., Zhu, L., Kim, P. S., Miller, C. C., Fisher, J. A., Travis, K., Yu, K., Hanisco, T. F., Wolfe, G. M., Arkinson, H. L., Pye, H. O. T., Froyd, K. D., Liao, J., and McNeill, V. F.: Aqueous-phase mechanism for secondary organic aerosol formation from isoprene: application to the southeast United States and co-benefit of SO_2 emission controls, Atmos. Chem. Phys., 16, 1603–1618, https://doi.org/10.5194/acp-16-1603-2016, 2016.

Marais, E. A., Jacob, D. J., Turner, J. R., and Mickley, L. J.: Evidence of 1991–2013 decrease of biogenic secondary organic aerosol in response to SO_2 emission controls, Environ. Res. Lett., 12, 054018, https://doi.org/10.1088/1748-9326/aa69c8, 2017.

Miao, R., Chen, Q., Shrivastava, M., Chen, Y., Zhang, L., Hu, J., Zheng, Y., and Liao, K.: Process-based and observation-constrained SOA simulations in China: the role of semivolatile and intermediate-volatility organic compounds and OH levels, Atmos. Chem. Phys., 21, 16183–16201, https://doi.org/10.5194/acp-21-16183-2021, 2021.

Ng, A. E., Chen, Y., Green, J., Farrell, S., Surratt, J. D., Ault, A. P., Turpin, B. J., and Vizuete, W. C.: Regional-scale modeling parameterizations for secondary organic aerosol formation from isoprene epoxydiols: experimentally based evaluation and optimization, ACS ES&T Air, 2, 2625–2637, https://doi.org/10.1021/acsestair.5c00258, 2025.

Nguyen, T. B., Bates, K. H., Crounse, J. D., Schwantes, R. H., Zhang, X., Kjaergaard, H. G., Surratt, J. D., Lin, P., Laskin, A., Seinfeld, J. H., and Wennberg, P. O.: Mechanism of the hydroxyl radical oxidation of methacryloyl peroxynitrate (MPAN) and its pathway toward secondary organic aerosol formation in the atmosphere, Phys. Chem. Chem. Phys., 17, 17914–17926, https://doi.org/10.1039/c5cp02001h, 2015.

Odum, J. R., Hoffmann, T., Bowman, F., Collins, D., Flagan, R. C., and Seinfeld, J. H.: Gas/particle partitioning and secondary organic aerosol yields, Environ. Sci. Technol., 30, 2580–2585, https://doi.org/10.1021/es950943+, 1996.

OpenAI: ChatGPT image-generation tools, OpenAI, available at: https://chatgpt.com/ (last access: 2 June 2026), 2026.

Paulot, F., Crounse, J. D., Kjaergaard, H. G., Kroll, J. H., Seinfeld, J. H., and Wennberg, P. O.: Isoprene photooxidation: new insights into the production of acids and organic nitrates, Atmos. Chem. Phys., 9, 1479–1501, https://doi.org/10.5194/acp-9-1479-2009, 2009a.

Paulot, F., Crounse, J. D., Kjaergaard, H. G., Kürten, A., St. Clair, J. M., Seinfeld, J. H., and Wennberg, P. O.: Unexpected Epoxide Formation in the Gas-Phase Photooxidation of Isoprene, Science, 325, 730–733, https://doi.org/10.1126/science.1172910, 2009b.

Pye, H. O. T. and Seinfeld, J. H.: A global perspective on aerosol from low-volatility organic compounds, Atmos. Chem. Phys., 10, 4377–4401, https://doi.org/10.5194/acp-10-4377-2010, 2010.

Pye, H. O. T., Pinder, R. W., Piletic, I. R., Xie, Y., Capps, S. L., Lin, Y.-H., Surratt, J. D., Zhang, Z., Gold, A., Luecken, D. J., Hutzell, W. T., Jaoui, M., Offenberg, J. H., Kleindienst, T. E., Lewandowski, M., and Edney, E. O.: Epoxide pathways improve model predictions of isoprene markers and reveal key role of acidity in aerosol formation, Environ. Sci. Technol., 47, 11056–11064, https://doi.org/10.1021/es402106h, 2013.

Pye, H. O. T., Zuend, A., Fry, J. L., Isaacman-VanWertz, G., Capps, S. L., Appel, K. W., Foroutan, H., Xu, L., Ng, N. L., and Goldstein, A. H.: Coupling of organic and inorganic aerosol systems and the effect on gas–particle partitioning in the southeastern US, Atmos. Chem. Phys., 18, 357–370, https://doi.org/10.5194/acp-18-357-2018, 2018.

Rattanavaraha, W., Chu, K., Budisulistiorini, S. H., Riva, M., Lin, Y.-H., Edgerton, E. S., Baumann, K., Shaw, S. L., Guo, H., King, L., Weber, R. J., Neff, M. E., Stone, E. A., Offenberg, J. H., Zhang, Z., Gold, A., and Surratt, J. D.: Assessing the impact of anthropogenic pollution on isoprene-derived secondary organic aerosol formation in $PM_{2.5}$ collected from the Birmingham, Alabama, ground site during the 2013 Southern Oxidant and Aerosol Study, Atmos. Chem. Phys., 16, 4897–4914, https://doi.org/10.5194/acp-16-4897-2016, 2016.

Riva, M., Chen, Y., Zhang, Y., Lei, Z., Olson, N. E., Boyer, H. C., Narayan, S., Yee, L. D., Green, H. S., Cui, T., Zhang, Z., Baumann, K., Fort, M., Edgerton, E., Budisulistiorini, S. H., Rose, C. A., Ribeiro, I. O., E Oliveira, R. L., Dos Santos, E. O., Machado, C. M. D., Szopa, S., Zhao, Y., Alves, E. G., De Sá, S. S., Hu, W., Knipping, E. M., Shaw, S. L., Duvoisin Junior, S., De Souza, R. A. F., Palm, B. B., Jimenez, J.-L., Glasius, M., Goldstein, A. H., Pye, H. O. T., Gold, A., Turpin, B. J.,

Vizuete, W., Martin, S. T., Thornton, J. A., Dutcher, C. S., Ault, A. P., and Surratt, J. D.: Increasing Isoprene Epoxydiol-to-Inorganic Sulfate Aerosol Ratio Results in Extensive Conversion of Inorganic Sulfate to Organosulfur Forms: Implications for Aerosol Physicochemical Properties, Environ. Sci. Technol., 53, 8682–8694, https://doi.org/10.1021/acs.est.9b01019, 2019.

Robinson, A. L., Donahue, N. M., Shrivastava, M. K., Weitkamp, E. A., Sage, A. M., Grieshop, A. P., Lane, T. E., Pierce, J. R., and Pandis, S. N.: Rethinking organic aerosols: semivolatile emissions and photochemical aging, Science, 315, 1259–1262, https://doi.org/10.1126/science.1133061, 2007.

Schmedding, R., Ma, M., Zhang, Y., Farrell, S., Pye, H. O. T., Chen, Y., Wang, C., Rasool, Q. Z., Budisulistiorini, S. H., Ault, A. P., Surratt, J. D., and Vizuete, W.: α-Pinene-Derived organic coatings on acidic sulfate aerosol impacts secondary organic aerosol formation from isoprene in a box model, Atmos. Environ., 213, 456–462, https://doi.org/10.1016/j.atmosenv.2019.06.005, 2019.

Schmedding, R., Rasool, Q. Z., Zhang, Y., Pye, H. O. T., Zhang, H., Chen, Y., Surratt, J. D., Lopez-Hilfiker, F. D., Thornton, J. A., Goldstein, A. H., and Vizuete, W. C.: Predicting secondary organic aerosol phase state and viscosity and its effect on multiphase chemistry in a regional-scale air quality model, Atmos. Chem. Phys., 20, 8201–8225, https://doi.org/10.5194/acp-20-8201-2020, 2020.

Schwantes, R. H., Charan, S. M., Bates, K. H., Huang, Y., Nguyen, T. B., Mai, H., Kong, W., Flagan, R. C., and Seinfeld, J. H.: Low-volatility compounds contribute significantly to isoprene secondary organic aerosol (SOA) under high-NOx conditions, Atmos. Chem. Phys., 19, 7255–7278, https://doi.org/10.5194/acp-19-7255-2019, 2019.

Schwantes, R. H., Emmons, L. K., Orlando, J. J., Barth, M. C., Tyndall, G. S., Hall, S. R., Ullmann, K., St. Clair, J. M., Blake, D. R., Wisthaler, A., and Bui, T. P. V.: Comprehensive isoprene and terpene gas-phase chemistry improves simulated surface ozone in the southeastern US, Atmos. Chem. Phys., 20, 3739–3776, https://doi.org/10.5194/acp-20-3739-2020, 2020.

Shrivastava, M., Andreae, M. O., Artaxo, P., Barbosa, H. M. J., Berg, L. K., Brito, J., Ching, J., Easter, R. C., Fan, J., Fast, J. D., Feng, Z., Fuentes, J. D., Glasius, M., Goldstein, A. H., Alves, E. G., Gomes, H., Gu, D., Guenther, A., Jathar, S. H., Kim, S., Liu, Y., Lou, S., Martin, S. T., McNeill, V. F., Medeiros, A., De Sá, S. S., Shilling, J. E., Springston, S. R., Souza, R. A. F., Thornton, J. A., Isaacman-VanWertz, G., Yee, L. D., Ynoue, R., Zaveri, R. A., Zelenyuk, A., and Zhao, C.: Urban pollution greatly enhances formation of natural aerosols over the Amazon rainforest, Nat. Commun., 10, 1046, https://doi.org/10.1038/s41467-019-08909-4, 2019.

Shrivastava, M., Rasool, Q. Z., Zhao, B., Octaviani, M., Zaveri, R. A., Zelenyuk, A., Gaudet, B., Liu, Y., Shilling, J. E., Schneider, J., Schulz, C., Zöger, M., Martin, S. T., Ye, J., Guenther, A., Souza, R. F., Wendisch, M., and Pöschl, U.: Tight Coupling of Surface and In-Plant Biochemistry and Convection Governs Key Fine Particulate Components over the Amazon Rainforest, ACS Earth Space Chem., 6, 380–390, https://doi.org/10.1021/acsearthspacechem.1c00356, 2022.

Silver, B., Conibear, L., Reddington, C. L., Knote, C., Arnold, S. R., and Spracklen, D. V.: Pollutant emission reductions deliver decreased $PM_{2.5}$-caused mortality across China during 2015–2017, Atmos. Chem. Phys., 20, 11683–11695, https://doi.org/10.5194/acp-20-11683-2020, 2020.

Stadtler, S., Kühn, T., Schröder, S., Taraborrelli, D., Schultz, M. G., and Kokkola, H.: Isoprene-derived secondary organic aerosol in the global aerosol–chemistry–climate model ECHAM6.3.0–HAM2.3–MOZ1.0, Geosci. Model Dev., 11, 3235–3260, https://doi.org/10.5194/gmd-11-3235-2018, 2018.

Su, S., Li, B., Cui, S., and Tao, S.: Sulfur Dioxide Emissions from Combustion in China: From 1990 to 2007, Environ. Sci. Technol., 45, 8403–8410, https://doi.org/10.1021/es201656f, 2011.

Surratt, J. D., Chan, A. W. H., Eddingsaas, N. C., Chan, M., Loza, C. L., Kwan, A. J., Hersey, S. P., Flagan, R. C., Wennberg, P. O., and Seinfeld, J. H.: Reactive intermediates revealed in secondary organic aerosol formation from isoprene, Proc. Natl. Acad. Sci. USA, 107, 6640–6645, https://doi.org/10.1073/pnas.0911114107, 2010.

Surratt, J. D., Gómez-González, Y., Chan, A. W. H., Vermeylen, R., Shahgholi, M., Kleindienst, T. E., Edney, E. O., Offenberg, J. H., Lewandowski, M., Jaoui, M., Maenhaut, W., Claeys, M., Flagan, R. C., and Seinfeld, J. H.: Organosulfate Formation in Biogenic Secondary Organic Aerosol, J. Phys. Chem. A, 112, 8345–8378, https://doi.org/10.1021/jp802310p, 2008.

Surratt, J. D., Kroll, J. H., Kleindienst, T. E., Edney, E. O., Claeys, M., Sorooshian, A., Ng, N. L., Offenberg, J. H., Lewandowski, M., Jaoui, M., Flagan, R. C., and Seinfeld, J. H.: Evidence for Organosulfates in Secondary Organic Aerosol, Environ. Sci. Technol., 41, 517–527, https://doi.org/10.1021/es062081q, 2007.

Tilmes, S., Hodzic, A., Emmons, L. K., Mills, M. J., Gettelman, A., Kinnison, D. E., Park, M., Lamarque, J. -F., Vitt, F., Shrivastava, M., Campuzano-Jost, P., Jimenez, J. L., and Liu, X.: Climate Forcing and Trends of Organic Aerosols in the Community Earth System Model (CESM2), J. Adv. Model. Earth Syst., 11, 4323–4351, https://doi.org/10.1029/2019MS001827, 2019.

Wennberg, P. O., Bates, K. H., Crounse, J. D., Dodson, L. G., McVay, R. C., Mertens, L. A., Nguyen, T. B., Praske, E., Schwantes, R. H., Smarte, M. D., St Clair, J. M., Teng, A. P., Zhang, X., and Seinfeld, J. H.: Gas-Phase Reactions of Isoprene and Its Major Oxidation Products, Chem. Rev., 118, 3337–3390, https://doi.org/10.1021/acs.chemrev.7b00439, 2018.

Worton, D. R., Surratt, J. D., LaFranchi, B. W., Chan, A. W. H., Zhao, Y., Weber, R. J., Park, J.-H., Gilman, J. B., De Gouw, J., Park, C., Schade, G., Beaver, M., Clair, J. M. St., Crounse, J., Wennberg, P., Wolfe, G. M., Harrold, S., Thornton, J. A., Farmer, D. K., Docherty, K. S., Cubison, M. J., Jimenez, J.-L., Frossard, A. A., Russell, L. M., Kristensen, K., Glasius, M., Mao, J., Ren, X., Brune, W., Browne, E. C., Pusede, S. E., Cohen, R. C., Seinfeld, J. H., and Goldstein, A. H.: Observational Insights into Aerosol Formation from Isoprene, Environ. Sci. Technol., 47, 11403–11413, https://doi.org/10.1021/es4011064, 2013.

Wu, K., Yang, X., Chen, D., Gu, S., Lu, Y., Jiang, Q., Wang, K., Ou, Y., Qian, Y., Shao, P., and Lu, S.: Estimation of biogenic VOC emissions and their corresponding impact on ozone and secondary organic aerosol formation in China, Atmos. Res., 231, 104656, https://doi.org/10.1016/j.atmosres.2019.104656, 2020.

Yang, Q., Yuan, Q., Li, T., Shen, H., and Zhang, L.: The relationships between $PM_{2.5}$ and meteorological factors in China: seasonal and regional variations, Int. J. Environ. Res. Public Health, 14, 1510, https://doi.org/10.3390/ijerph14121510, 2017.

Zaveri, R. A., Easter, R. C., Fast, J. D., and Peters, L. K.: Model for Simulating Aerosol Interactions and Chemistry (MOSAIC), J. Geophys. Res., 113, 2007JD008782, https://doi.org/10.1029/2007JD008782, 2008.

Zaveri, R. A., Easter, R. C., Singh, B., Wang, H., Lu, Z., Tilmes, S., Emmons, L. K., Vitt, F., Zhang, R., Liu, X., Ghan, S. J., and Rasch, P. J.: Development and Evaluation of Chemistry-Aerosol-Climate Model CAM5-Chem-MAM7-MOSAIC: Global Atmospheric Distribution and Radiative Effects of Nitrate Aerosol, J. Adv. Model. Earth Syst., 13, e2020MS002346, https://doi.org/10.1029/2020MS002346, 2021.

Zawadowicz, M. A., Lee, B. H., Shrivastava, M., Zelenyuk, A., Zaveri, R. A., Flynn, C., Thornton, J. A., and Shilling, J. E.: Photolysis controls atmospheric budgets of biogenic secondary organic aerosol, Environ. Sci. Technol., 54, 3861–3870, https://doi.org/10.1021/acs.est.9b07051, 2020.

Zhang, G. J. and McFarlane, N. A.: Sensitivity of climate simulations to the parameterization of cumulus convection in the Canadian climate centre general circulation model, Atmosphere-Ocean, 33, 407–446, https://doi.org/10.1080/07055900.1995.9649539, 1995.

Zhang, W., Liu, Y., Yue, M., Dong, X., Huang, K., and Wang, M.: Understanding the long-term trend of organic aerosol and the influences from anthropogenic emission and regional climate change in China, Atmos. Chem. Phys., 25, 3857–3872, https://doi.org/10.5194/acp-25-3857-2025, 2025.

Zhang, Y., Chen, Y., Lambe, A. T., Olson, N. E., Lei, Z., Craig, R. L., Zhang, Z., Gold, A., Onasch, T. B., Jayne, J. T., Worsnop, D. R., Gaston, C. J., Thornton, J. A., Vizuete, W., Ault, A. P., and Surratt, J. D.: Effect of the Aerosol-Phase State on Secondary Organic Aerosol Formation from the Reactive Uptake of Isoprene-Derived Epoxydiols (IEPOX), Environ. Sci. Technol. Lett., 5, 167–174, https://doi.org/10.1021/acs.estlett.8b00044, 2018.

Zhang, Y., Chen, Y., Lei, Z., Olson, N. E., Riva, M., Koss, A. R., Zhang, Z., Gold, A., Jayne, J. T., Worsnop, D. R., Onasch, T. B., Kroll, J. H., Turpin, B. J., Ault, A. P., and Surratt, J. D.: Joint impacts of acidity and viscosity on the formation of secondary organic aerosol from isoprene epoxydiols (IEPOX) in phase-separated particles, ACS Earth Space Chem., 3, 2646–2658, https://doi.org/10.1021/acsearthspacechem.9b00209, 2019.

Zhang, Y.-Q., Ding, X., He, Q.-F., Wen, T.-X., Wang, J.-Q., Yang, K., Jiang, H., Cheng, Q., Liu, P., Wang, Z.-R., He, Y.-F., Hu, W.-W., Wang, Q.-Y., Xin, J.-Y., Wang, Y.-S., and Wang, X.-M.: Observational Insights into Isoprene Secondary Organic Aerosol Formation through the Epoxide Pathway at Three Urban Sites from Northern to Southern China, Environ. Sci. Technol., 56, 4795–4805, https://doi.org/10.1021/acs.est.1c06974, 2022.

Zheng, Y., Thornton, J. A., Ng, N. L., Cao, H., Henze, D. K., McDuffie, E. E., Hu, W., Jimenez, J. L., Marais, E. A., Edgerton, E., and Mao, J.: Long-term observational constraints of organic aerosol dependence on inorganic species in the southeast US, Atmos. Chem. Phys., 20, 13091–13107, https://doi.org/10.5194/acp-20-13091-2020, 2020.

Zhu, S., Zhang, J., Li, L., Zhou, M., Qiao, L., Wang, H., Huang, D. D., Wang, Q., Jing, S., Wu, Y., Wang, S., Chen, C., Ying, Q., and Yu, J. Z.: Aerosol Uptake Coefficients of Isoprene Epoxides: Determination and Parameter Estimation from Online Field Measurements of Organic Molecular Markers, Environ. Sci. Technol., 59, 18249–18258, https://doi.org/10.1021/acs.est.5c09046, 2025.

1140